TURKISH NAVAL ACADEMY
NAVAL SCIENCE AND ENGINEERING INSTITUTE
DEPARTMENT OF COMPUTER ENGINEERING
MASTER OF SCIENCE PROGRAM
IN COMPUTER ENGINEERING

EVALUATION OF FIGHTER EVASIVE MANEUVERS AGAINST PROPORTIONAL NAVIGATION MISSILES

Master Thesis

REMZİ AKDAĞ

Advisor: Assist.Prof. D.Turgay Altılar

İstanbul, 2005

CERTIFICATE OF COMMITTEE APPROVAL

EVALUATION OF FIGHTER EVASIVE MANEUVERS AGAINST PROPORTIONAL NAVIGATION MISSILES

Submitted in partial fulfillment of the requirements for degree of

MASTER OF SCIENCE IN COMPUTER ENGINEERING
from the

TURKISH NAVAL ACADEMY

Author:

_____

Remzi Akdağ

Defense Date : 13 / 07 / 2005
Approved by : 13 / 07 / 2005

_____

Assist.Prof. Deniz Turgay Altılar (Advisor)

_____

Prof. Ercan Öztemel (Defense Committee Member)

_____

Assoc.Prof. Coşkun Sönmez (Defense Committee Member)

ABSTRACT (TURKISH)

SAVAŞ UÇAKLARININ ORANTISAL SEYİR YAPAN GÜDÜMLÜ MERMİLERDEN SAKINMA MANEVRALARININ DEĞERLENDİRİLMESİ

Anahtar Kelimeler : Orantısal seyir, sakınma manevraları, aerodinamik kuvvetler

Bu tezde, orantısal seyir adı verilen güdüm sistemiyle ilerleyen güdümlü mermilere karşı uçaklar tarafından icra edilen sakınma manevralarının etkinliği ölçülmüş, farklı güdümlü mermilerden kaçış için en uygun manevralar tanımlanmıştır. Uçuş aerodinamikleri, matematiksel modele bir temel oluşturmak amacıyla sunulmuştur. Bir hava savaşında güdümlü mermilerden sakınmak için uçaklar tarafından icra edilen belli başlı manevraların matematiksel modelleri çıkarılıp uygulanılmış, görsel simülasyonu gerçekleştirilmiş ve bu manevraların değişik başlangıç değerlerine göre başarım çözümlemeleri yapılmıştır. Güdümlü mermi-uçak karşılaşma senaryolarında güdümlü merminin terminal güdüm aşaması ele alınmıştır. Gerçekçi çözümleme sonuçları elde edebilmek amacıyla uçuş aerodinamiklerinin göz önüne alınmasıyla elde edilen yönlendirme kinematiklerini içeren genişletilmiş nokta kütleli uçak modeli kullanılmıştır. Çalışmamızda yaptığımız çözümleme sonucunda, değişik karşılaşma senaryolarında, hangi manevranın güdümlü mermiden daha etkin olarak sakınma sağlayacağı konusunda fikir verilmektedir.

Uçak modellerinde kullanılan parametreler yüksek-g kabiliyetine sahip savaş uçaklarının özelliklerine yakın genel değerlerdir.

ABSTRACT (ENGLISH)

EVALUATION OF FIGHTER EVASIVE MANEUVERS AGAINST PROPORTIONAL NAVIGATION MISSILES

Keywords: Proportional Navigation, Evasive maneuvers, aerodynamic forces.

In thesis, evasive maneuvers of a fighter against a missile employing proportional navigation are measured. Flight kinematics and flight dynamics are represented in order to constitute a basis for the fighter model. Notable evasive maneuvers performed by a fighter aircraft against proportional navigation missiles in an air combat are extracted, implemented visually simulated and performance analyses of these maneuvers are made with respect to different initial parameters. The terminal phase of the encounter is taken into consideration. An extended point-mass aircraft model including orientation kinematics is used to obtain realistic results. After gathering performance analysis results for various missile-aircraft encounter scenarios, we put forward an idea about which maneuver will provide for an effective evasion from the guided missiles.

The parameters used for the fighter models represent generic fighter aircraft with high-g capability.

DISCLAIMER STATEMENT

The views expressed in this thesis are those of the author and do not reflect the official policy or position of the Turkish Navy, Naval Academy, and Naval Science and Engineering Institute.

DEDICATION

To my mom, dad, sister and brother.

ACKNOWLEDGMENTS

I wish to extend my sincere appreciation and gratitude to my advisor Assist.Prof. D.Turgay Altılar for his guidance, assistance, encouragement, and friendship. His determination and confidence to success always gave endurance to me when I face difficulties during my studies.

I would like to extend my appreciation to Lt.Mustafa DİNÇ for sharing his knowledge and resources with me.

I would like to thank Prof.Süleyman Özkaynak, Assist.Prof.Vedat Coşkun, and personnel of Naval Science and Engineering Institute for their support.

Finally, I would like to thank my friend İnanç Moran. In the future, I believe that two of us will carry out many studies on missile guidance.

TABLE OF CONTENTS

LIST OF FIGURES

LIST OF TABLES

LIST OF ABBREVIATIONS, ACRONYMS, AND SYMBOLS

2D	Two Dimensional
3D	Three Dimensional
BFM	Basic Fighter Maneuvers
CG	Center of Gravity
ECM	Electronic Counter Measures
HGB	High-g Barrel Roll
HUD	Heads Up Display
ICAO	International Civil Aviation Organization
LOS	Line of Sight
NASA	National Aeronautics and Space Administration
VEGAS	Visual End Game Simulation
VIATO	Visual Interactive Aircraft Trajectory Optimization
a	Velocity of Sound
aoa	Angle of Attack
$\mathcal{A}$	Aerodynamic Forces
$\mathcal{A}_C$	Cross Sectional Area of the Stream Tube of an Aircraft Engine
$\mathcal{AR}$	Aspect Ratio
b	Wing Span
C_D	Drag Coefficient
C_{D0}	Zero-Lift Drag Coefficient
C_{Di}	Lift-Induced Drag Coefficient
C_{Dwave}	Wave-Induced Drag Coefficient
C_f	Skin Friction Coefficient
$const$	Constant
$c_{l\alpha}$	Two Dimensional Airfoil Lift Curve Slope
C_L	Lift Coefficient
C_{Lo}	Zero-Lift Coefficient
$C_{L\alpha}$	Three Dimensional Finite Wing Lift Curve Slope
$\mathcal{D}$	Drag Force
e_o	Oswald's Efficiency Factor
$\mathcal{E}$	Lift-to-Drag Ratio, Aerodynamic Efficiency
$\mathcal{E}_{max}$	Maximum Lift-to-Drag Ratio
F	Force
g	Acceleration of Gravity
h	Altitude

$\mathcal{L}$	Lift Force
m	mass
$\mathcal{M}$	Mach Number
n	Load Factor
n_c	Acceleration Command
nr	Mass Flow Rate
$\mathcal{N}'$	Effective Navigation Ratio
$\boldsymbol{P}$	Pitch Rate
q	Dynamic Pressure
$\boldsymbol{r}$	Turn Radius
$\mathcal{S}$	Reference Area of the Wing
$\mathcal{S}_{wet}$	Wetted Area
$\mathcal{T}$	Thrust Force
$\mathcal{T}_{max}$	Maximum Available Thrust
$\mathcal{T}_{SL}$	Thrust at Sea Level
u	Throttle Setting (Proportion of Maximum Thrust Used)
$\mathcal{V}$	Velocity
$\mathcal{V}_a$	Maneuvering Speed
$\mathcal{V}_m$	Velocity of the Missile
$\mathcal{V}_t$	Velocity of the Target
$\mathcal{W}$	Weight
X	Range (x-axis)
Y	Range (y-axis)
α	Angle of Attack
$\alpha_{\mathcal{T}}$	Thrust Angle
γ	Flight Path Angle
$\dot{\lambda}$	Line-of-Sight Rate
Λ_{LE}	Sweep Angle on the Leading Edge of the Wing
μ	Bank Angle
ρ	Air Density
ρ_{SL}	Air Density at Sea Level
χ	Heading Angle
χ_{m}	Initial Heading Angle of the Missile
χ_{t}	Initial Heading Angle of the Target
w	Turn Rate

I. INTRODUCTION

Since the end of World War II, many different methods for missile guidance have been developed to successfully intercept a stationary, predictable, or even highly maneuvering target [1]. As an expected result of tactical homing missiles' revealing in 1944, it became an obligation to develop target evasive maneuvering tactics against pursuers. This thesis considers the evasive maneuvers of highly maneuvering targets, so called the fighters.

This work is part of a joint project. The joint project is in view of an air combat, particularly, the last seconds of an air combat when an air-to-air missile is launched. The attitudes of the fighter during the missile-fighter encounter are considered in this thesis.

A. FIGHTER EVASIVE MANEUVERS

The performance of guidance systems can generally be quantified in terms of the miss distance between the missile and the target. Miss distance is the difference between the target and missile lateral displacements with respect to the reference line of sight (LOS). From a target's point of view, an optimal maneuver means techniques that provide the target with long intercept time and large miss distance.

In the evasion problem, there are two objects of interest: a fighter and a missile maneuvering in a three-dimensional world. The aim of the pilot is to control the turning rate of the plane to avoid being hit by the approaching missile. The missile tracks the motion of the plane and steers toward the plane's anticipated position [3]. The initial speed of the missile is greater than that of the plane, but the missile loses speed as it maneuvers. If the missile speed drops below some threshold, it loses maneuverability and drops out of the sky. The more the fighter aircraft maneuvers effectively, the more miss distance and longer intercept time is provided.

Since the proportional navigation –in which the missile turning rate is made proportional to the line of sight rate- is the most broadly used guidance method due to its effectiveness, target evasive maneuvers against proportionally navigating guided missiles are investigated in this study. The implementation of proportional navigation guidance system proposed by Moran [2] and Moran and Altilar [4] is used as the pursuing missile's guidance system.

So far, many methods have been studied on optimal maneuvers of an aircraft evading from a proportional navigation guided missile. Some of numerically obtained optimal maneuvers are barrel roll, split-s, and horizontal-s maneuvers.

Although aforesaid maneuvers are numerically accepted, there are many avoidance methods that are performed by fighter pilots under missile threats. Since practicing evasion tactics are quite expensive and time consuming tasks, creating mathematical models and evaluating the performance of other evasive methods are inevitable. Motivated by this fact, a number of notable maneuvers, such as break turn, barrel roll, Immelmann, split-s, horizontal-s and their combinations are studied.

B. AERODYNAMICS AND KINEMATICS

The terminal phase of a missile-aircraft encounter takes 5-10 seconds. In this short period of time the pilot must choose the convenient maneuver by considering the characteristics of the aircraft and possibly the missile, and perform it. So, in an endgame maneuvering, the rotation of the aircraft plays a significant role. Neglecting the aerodynamic forces and the orientation kinematics while modeling the most crucial phase of a missile-aircraft encounter scenario will contradicts the reality. Consequently, if realistic evaluation of the effectiveness of the performed maneuvers is desired, aerodynamic forces must be taken into account.

Based on the above considerations, conventional point-mass model is extended to include bank angle and angle of attack. This inclusion yields finite angular velocity around the pitch and the roll axes. The limited forces and torques provided by the aerodynamic actuators cause the finite velocities.

C. SIMULATION ENVIRONMENT

To evaluate the motions of a fighter aircraft and the fighter evasive maneuvers against proportional navigation, new software that is called Visual End-Game Simulation (VEGAS) has been developed. All the factors required for gathering realistic results, i.e. aircraft specifications, aerodynamics, kinematics, and notable evasive maneuvers of fighters, are included in this software. On the other hand, the required factors relevant to the missile employing proportional navigation are included in VEGAS. Also the modular structure of the software has made it completely apt to further developments, such as, adding electronic counter-measures (ECM), radar limitations for both the missile and the aircraft, new evasive maneuvers.

By using this new software, extensive simulation results that are supported by comprehensible visual projections have been obtained. Visual C++ and Open GL are used in simulations. OpenGL's main purpose is to render two and three-dimensional objects into a frame buffer [31]. A 3D visualization is performed in order to provide the user for a comprehensive understanding about the terminal phase of the encounter.

C. CONTRIBUTION OF THIS THESIS

In this thesis, the evasive maneuvers performed by a fighter aircraft against proportional navigation missiles are evaluated via a software program developed in the Naval Science and Engineering Institute. With this software, supplying it with the required aircraft-specific data and with the initial conditions, it is possible to analyze simply the attitudes of that aircraft when it performs different

maneuvers, or analyze the performance of its evasive maneuvers against a proportional navigation.

So, the result of this study;

- may be used by pilot training associations for training purposes,

- may be used as a tool to analysis the performance of any kind of aircraft,

- in the future, may be attached to a joint combat simulation which includes air, navy, army combat.

D. STRUCTURE OF THIS THESIS

After giving a brief introduction about this thesis in Chapter I, we reviewed the literature considering evasive maneuvers against proportional navigation missiles, and surveyed investigate the background information about the basic fighter maneuvers, the aerodynamics and kinematics in Chapter II. This background information constitutes the basis of this thesis, i.e. what we consider for performance analyses, and how we take those considerations into account.

In Chapter III, the definition of the Visual End-Game Simulation (VEGAS) software -which we've developed in the Naval Science and Engineering Institute-, is given.

Performance evaluations for sample missile-fighter encounter scenarios are made in Chapter IV.

Finally, we conclude the thesis in Chapter V.

II. RELATED WORK AND BACKGROUND

In this chapter, the related work about the aircraft simulation and the evasive maneuvers of the fighter aircraft is briefly surveyed. Afterwards, the theme known as the Basic Fighter Maneuvers (BFM) which entirely deals with the maneuvers of fighter aircraft in an air combat is given in details, and the evasive maneuvers that are modeled in this thesis are defined. Finally, the topics of kinematics and aerodynamics which considers the motions of a fighter aircraft are exclusively focused on.

A. REVIEW OF RELATED WORK

Many methods on fighter evasive maneuvers against missiles have been studied over the last six decades. Most of these studies related to finding optimal maneuvers and trajectories of aircraft evading from missiles.

Choi et al. (2001) considered three-dimensional target optimal evasion problem against a proportionally guided missile [5]. They formulate the optimal evasion problem of an n aircraft as a constrained optimization problem whose payoff is the intercept time and constraint is the capture condition.

Optimal evasive control maximizing the miss distance for very simple two-dimensional missile and constant speed target was considered by Ben-Asher and Cliff (1989) [6].

Imado and Miwa (1986) represented the optimality of the horizontal-S maneuver when the final time and miss distance are taken as the cost function [7].

Imado and Uehara (1996) discussed the performance of the high-g barrel roll (HGB) maneuver from optimal control of view [8]. The mathematical model for three-dimensional pursuit-evasion problem of the aircraft against proportional navigation missile was considered; some features of the aircraft optimal evasive maneuvers, and high-g barrel roll maneuvers were explained. Finally, the exact numerical solution for the three-dimensional pursuit-evasion problem was

illustrated and the non-optimality of the HGB was shown. The relation between the optimal maneuver and the HGB was also discussed.

Minimum time trajectories to a fixed or moving target were produced with an MS compatible software called Visual Interactive Aircraft Trajectory Optimization (VIATO) by Virtanen et al. (1999) [9]. In this study, the authors introduced a new approach for the automated solution of optimal flight trajectories. The structure of the aircraft models and the objectives of the problems were specified, and different aircraft types were stored in their model library. The approach was implemented in the VIATO which consists of an optimization server, a model server, and an intuitive, menu-driven, graphical user interface.

Realistic target models including the variation of thrust and aerodynamic forces according to the Mach number were used by Ong and Pierson (1996) [10]. Their work is considering optimal evasive maneuvers against proportional missiles.

The optimal avoidance of a missile employing proportional navigation was dealt with in [11]. An extended point mass vehicle model including orientation kinematics was used to obtain realistic results. The drag, thrust and constraint data of vehicles represented a generic fighter aircraft and a medium range air-to-air missile.

Moore and Garcia [12] described the implementation of a genetic programming system that evolved optimized solutions to the extended two dimensional pursuer/evader problems that did not depend upon knowledge of pursuer’s current state.

A great number of pursuit-evasion simulations were conducted by giving both aircraft and missile the strategies for combinations of parameter spaces and initial conditions in [13]. Final miss distance was chosen as the performance index of the games; the missile tried to minimize it, while the aircraft tried to maximize it. According to this method, the basic idea laid in giving players a priori optimal

or suboptimal feedback strategies, conducting massive simulations in the parameter space of the initial geometries and guidance law parameters, and analyzing the results. In a later work [14], different approaches to pursuit-evasion were considered including the method in [13]. These approaches were:

- give both players some suboptimal feedback strategies and conduct a great number of Monte Carlo simulations,

- give one player a suboptimal feedback strategy and the other player an exact one-sided nonlinear optimal control,

- give both players suboptimal feedback strategies dependent on parameters.

National Aeronautics and Space Administration (NASA) developed a simulation that is capable of quickly and efficiently supporting flight research requirements and conceptual vehicle studies [15]. The simulations in this work operate on UNIX-based platforms and were coded with a FORTRAN shell and C support routines. This simulation software is still used at NASA, within industry, and at several universities, and applicable to a broad range of fixed-wing aircraft including fighters.

Another versatile aircraft simulation study made in the NASA [16] emphasized that realistic aircraft motion was of greatest importance, and accurate roll and pitch dynamics were very significant in developing evasive maneuvers against missiles.

B. BASIC FIGHTER MANEUVERS (BFM)

As the missiles and fighter aircraft become more advanced, and technology improves, the need for new air combat tactics, both offensive and defensive, becomes more crucial. While all the countries are trying to developing new tactics, they are training their pilots to maintain their combat readiness and improve their skills to successfully apply air tactics. Main goal of training is

clearly declared in an official air force documentary [17]: “FLY, FIGHT and WIN!” For a single pilot of a fighter aircraft, performing Basic Fighter Maneuvers (BFM) is the basis for achieving air combat duties. Consequently, for a fighter pilot, it’s crucial to understand the fundamentals of Basic Fighter Maneuvers.

1. Fundamentals of BFM

Angle off, range, and aspect angle terms are used in order to describe relative positions in BFM (see Fig. 1).

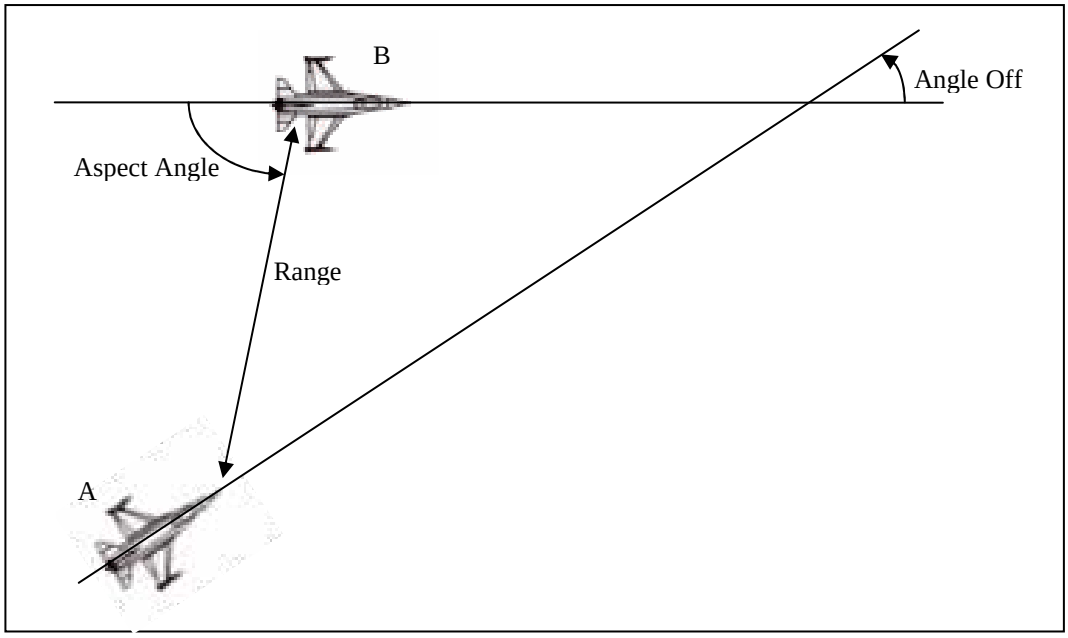

Figure 1.Angle off, Range, and Aspect Angle

a. Angle Off

Angle-off is the difference, measured in degrees, between the heading of the aircraft ‘A’ and ‘B’. If the angle-off is 0 degree, the fuselage of ‘A’ is parallel with the fuselage of ‘B’. ‘A’ is perpendicular to ‘B’ if angle off is 90 degrees.

b. Range

Range is simply the distance between the aircraft ‘A’ and the aircraft ‘B’, and can be represented in miles or feet. Most modern military aircraft HUD systems (Heads up Display) read in nautical miles and tenths of miles if the

aircraft is more than a mile from the opponent, after less than 1 mile is met, the display will read in feet.

c. Aspect Angle

Aspect angle is degrees from the tail of ‘B’ to ‘A’. This indicates the relative position. Aspect angle is not dependent of heading of the aircraft. So, the aspect angle won’t change with angle off. The aspect angle is zero when ‘A’ is on the tail of ‘B’. The nose of ‘B’ is 180 degrees. If ‘A’ is on the right of ‘B’, that is right aspect, vice versa. Tactical advantage in close-in air combat can be measured as the difference between the aspect angle of ‘B’ and aspect angle of ‘A’, since the most desirable condition for the attacker is to point directly at the target while the target is directly away from the attacker.[18]

2. Offensive BFM

Offensive BFM is the maneuvers to beat the opponent. The main objective of offensive BFM is to take the initiative of the encounter and obtaining appropriate position for the killing shot.

The best position to meet the main objectives of offensive BFM is being just behind the opponent (at six o’clock). In order to manage this, a pilot must keep control of the aforesaid values, angle-off, range, and aspect angle. When both angle-off and aspect angle are 0, the aircraft is at six o’clock of the opponent. Also, the pilot will need smooth turns to maintain this situation. That’s to say, sudden jerks, immediate directional changes will cause loss of energy, speed and attitude.

a. Energy

Energy is an important issue in BFM. Any aerial maneuver costs energy. An aircraft has two types of energy: potential and kinetic. Potential energy is proportional to the altitude, and kinetic energy is related to the speed. The higher a

fighter flies, the more energy is available for use. A pilot can trade potential energy for kinetic energy (speed), vice versa.

b. Turn Radius

Turn radius is the distance from the center of the turn to the turn circle of the aircraft. It is simply a measure of how tight the aircraft is turning. The simple equation for turn radius is

$$\boldsymbol{r} = \mathcal{V}^2 / n \tag{1}$$

where $\boldsymbol{r}$ is the turn radius, $\mathcal{V}$ is airspeed and n is load factor, the ratio of the lift to the weight. As stated by the equation, higher airspeed causes higher turn radius.

Load factor, n, is the lift-to-weight ratio and can be defined as the magnitude of lift force relative to the gravitational force and oriented by the rotation of the velocity vector. In normal, 1-g equilibrium flight, lift equals weight. The aircraft produces lift that is double of its weight in a 2-g turn. Also, this is an aircraft-specific quantity and defines the structural limit of an aircraft.

c. Turn Rate

Turn rate is the magnitude that specifies how fast the aircraft can move on the turn circle. The simple equation for the turn rate is

$$w = n / \mathcal{V} \tag{2}$$

where w, n, $\mathcal{V}$ is the turn rate, load factor and airspeed, respectively. Turn rate is measured in degrees and is dependent on the load factor and airspeed. So, high load factor and low airspeed increases maneuverability.

d. Maneuvering Speed

Maneuvering speed, $\mathcal{V}_a$, is the maximum speed at which an aircraft in symmetrical flight at the specified flight and configuration will stall before exceeding limit load and sustaining possible structural damage. Aircraft are

aerodynamically g-limited by the lift line up to maneuvering speed, and structurally g-limited by the load factor line above it. Figure 2 indicates the relationship between airspeed, maneuvering capability and the structural limit.

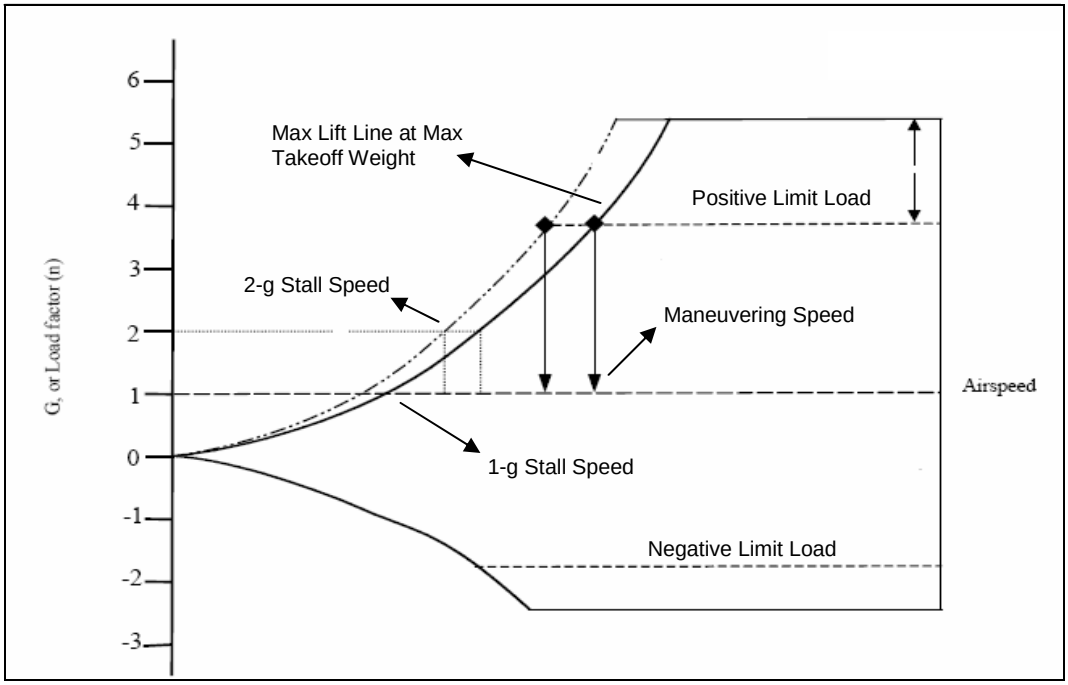

Figure 2.V-n Diagram

Maximum lift line indicates how thrust can be applied to change the flight path of the aircraft without stalling the wings or doing damage through excessive loads. As seen from Fig. 2, if the speed of the aircraft with 1-g load becomes less than the stall speed, the lift produced by the wings passes down the weight and its nose goes down. This is why an aircraft is aerodynamically g-limited by the lift line. In a turning maneuver, as the pitch rate is increased at a given airspeed, load factor increases until the maximum lift line is reached. At that point, airflow starts to separate from the wings and the fuselage starts to belabor the tails, and finally, structural damage occurs. This is why an aircraft is g-limited by the lift line.

Consequently, the definition of maneuvering speed is the maximum speed, at a given weight and configuration, at which anyone flight control surface

can be abruptly and fully deflected –not to include rapid control surface reversals- without causing aircraft damage. [19]

e. Corner Speed

Maneuvering speed is also known as the corner speed and can be briefly defined as the optimum speed at which the turn rate is maximized [20]. Practical values of corner speed of fighter aircraft range in 400-500 knots.

Turn radius goes to minimum at corner speed as the turn radius is proportional to V^2 / n. Therefore radius is minimized by high g and low airspeed. Corner speed is the lowest speed for the highest structural load factor.

Turn rate is proportional to n / V. Then, turn rate increases until corner speed is reached. Combinations of high g and low airspeed favor turn rate. Maneuvering at maximum structural g at any airspeed higher than the corner velocity causes lower turn rate.

To achieve the best turn rate and radius, airspeed must be controlled. There are four ways to control airspeed in a fighter:

- Throttle

- Drag devices

- Angle of Attack

- g Forces

Throttle position controls how much fuel is burned. Drag devices refer primarily to speed brakes. Nose position in relation to the horizon also affects airspeed. Finally, g force causes airspeed to bleed off. No modern fighter can stay at corner velocity while pulling max g's at medium altitude because of the energy trade-off discussed before. As pulling g's, aircraft will slow down. Starting

maneuvering close to corner velocity is important for controlling the energy consumption.

3. Defensive BFM

Defensive basic fighter maneuvers are performed when a fighter encounters an attacking fighter or a missile threat. In an encounter called a dogfight, the one on the defensive must perform defensive BFM to keep the opponent out of the “Kill Zone”.

The most basic defensive BFM method is to put the missile on the 3/9 line (see Fig. 3). As missiles employing proportional navigation guidance system flies to the prospective position of the evader in order to achieve maximum range, putting the missile on the 3/9 line causes it to make hard turns. After performing this maneuver, dropping chaff will confuse the missile as it tries to solve the guidance problem, and also it causes it to lose energy. This provides the pilot for some more time to take other evasive maneuvers. If it is too late for taking these measures, the method for evading is jinking which is a combination of random evasive maneuvers including high g turns and rolls. All the concepts, such as structural limits, for fighter maneuvers stated in previous sections must also be considered in defensive BFM.

Also it must be considered that the missiles are designed to explode if they overshoot the target. So, trying to keep the missile on the 3/9 line too long will reduce the range to the missile. When it gets close enough to explode, even if it’s going to overshoot, its fuse will be activated and it will explode. Some time before the missile gets that close, evasive maneuvers to break away the missile must be performed.

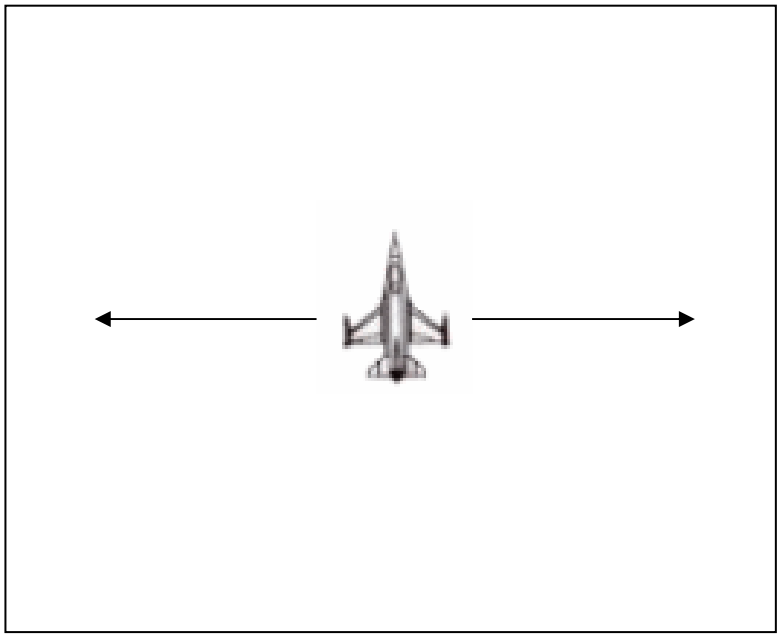

Figure 3.The 3/9 Line of a Fighter

In the next section, fighter evasive maneuvers that are studied in this thesis are defined.

a. Roll

This is the most basic maneuver to achieve all other turn maneuvers in BFM (see Fig. 4). A roll is performed by rotating the aircraft around the longitudinal axis by the use of stick to apply bank angle which is discussed in the next chapter. Longitudinal axis extends along the fuselage from tail to nose.

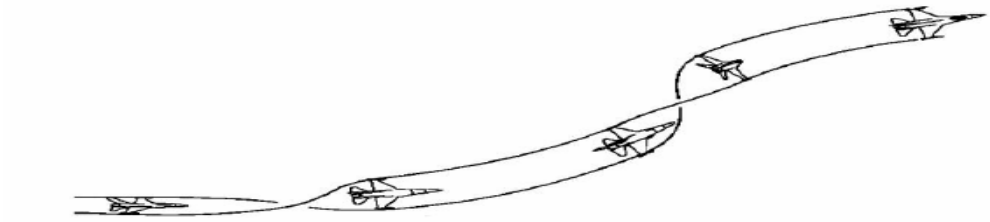

Figure 4.Roll Maneuver [22]

b. Break Turn

The break turn results in a tight turn with high roll angle (see Fig. 5). It is a defensive maneuver used to avoid a missile or, in a dogfight, to deny the opponent weapon employment opportunity when the opponent is behind the target (on the six). The point is to create as much angle as you can on the bandit. The break turn is a high energy consuming maneuver [22]. If this maneuver is performed repeatedly, then it becomes a horizontal-s maneuver and, is commonly performed against missiles.

If the target is equipped with radar warning system, the missile's lock-on to the target causes alarm which is typically the first evidence of an incoming threat. The target pilot may try to overcome the missile attack by making a hard break turn and diving [23, 24].

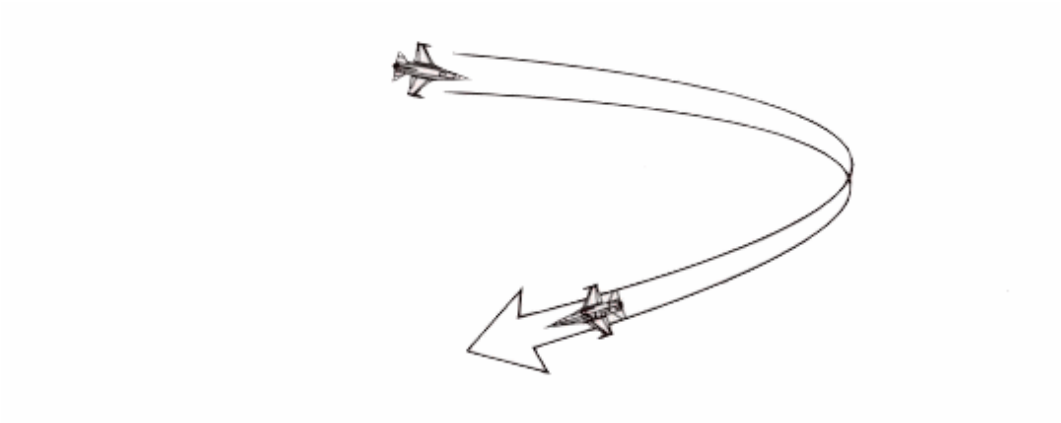

Figure 5.Break Turn

c. Barrel Roll

Similar to a roll, the pilot applies back pressure on the stick, i.e., changes the angle of attack) while he is rolling to the left or right. This makes the aircraft plane fly in a corkscrew pattern and is used to make the missile deal with one of the most difficult guidance problems because of its three dimensional nature. This maneuver can be performed both offensively and defensively. Defensive barrel roll maneuver is used to make the missile deal with the hardest guidance

problems. Because of its three dimensional nature, this maneuver produces high miss distances. Figure 6 shows the flight path of a fighter in a barrel roll maneuver.

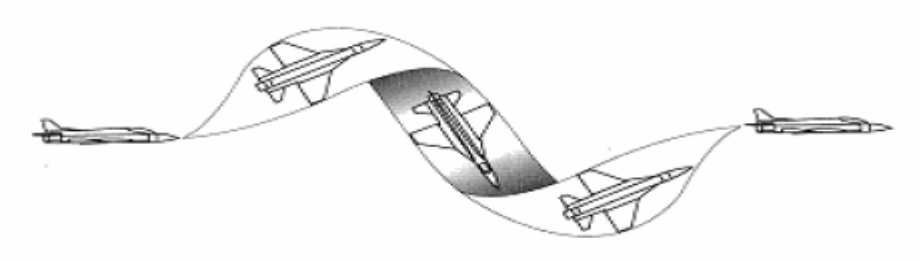

Figure 6.Barrel Roll Maneuver [22]

Although barrel roll is considered to be a successful maneuver to avoid missiles, its non-optimality is shown by Imado and Uehara [8]. They discuss the performance of the high-g barrel roll (HGB) against proportional navigation missiles from the perspective of optimal control. In their study, the exact numerical solution for the three-dimensional pursuit-evasion problem is illustrated and the non-optimality of the HGB is shown.

d. Immelmann Turn

The Immelmann Maneuver is named after Max Immelmann, a World War I German ace who reportedly invented the maneuver. The Immelmann is essentially a maneuver for repositioning. As the Immelmann is a very effective tool for setting up for an engagement used by attacker aircrafts, it also can be applied, rarely, in defensive situations. In this thesis, performance of Immelmann turn is studied because its opposition to the split-s maneuver. Basically, the Immelmann is a quick way to change direction while increasing altitude (see Fig. 7).

Figure 7.Immelmann Turn [22]

Back in 1916 the original Immelmann turn was more akin to the vertical reverse than its present-day counterpart. The modern version of the Immelmann is a vertical climb or half loop, possibly aileron-turning during the climb, then rolling out into level flight at the top. Its main value lies in using the vertical plane to change the direction of flight in the smallest possible horizontal space. Horizontal turns at normal fighting speeds take up a lot of room laterally. Using the vertical plane enables the fighter to turn square corners in relation to its position above the ground. This maneuver makes repositioning for meeting a threat, much easier than would be the case using horizontal maneuver only [25]. Note that kinetic energy of the aircraft is traded to the potential energy by performing this maneuver.

e. Split-s

The Split-s is the Immelmann in reverse, and consists of a half-roll followed by a partial loop under. One important prerequisite of this maneuver is a fairly high altitude. The turn begins with rolling 90 degrees; once upside down, pulling back on the stick to execute a vertical U-turn. By performing this maneuver, a pilot can reverse directions and gain a lot of speed. (See Fig. 8)

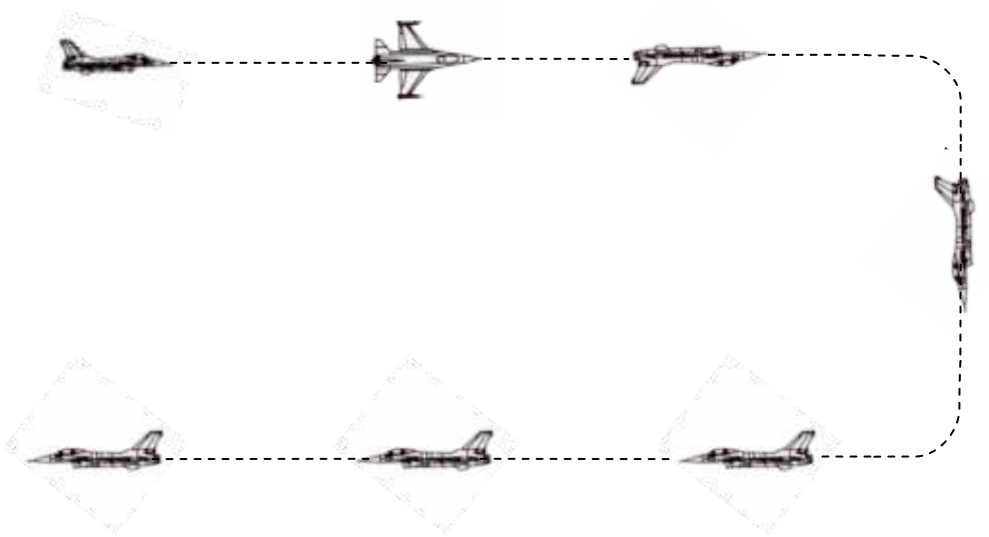

Figure 8.Split-s Maneuver

C. FLIGHT KINEMATICS AND AERODYNAMICS

1. Aerodynamic Forces on an Aircraft

There are four forces acting on an aircraft. These forces are represented for a climbing flight in the vertical plane in Figure 9. These are thrust, lift, drag and weight. The first two forces favor the motion of an aircraft. On the contrary, drag and weight are against the first two and have dissipative effects on motion.

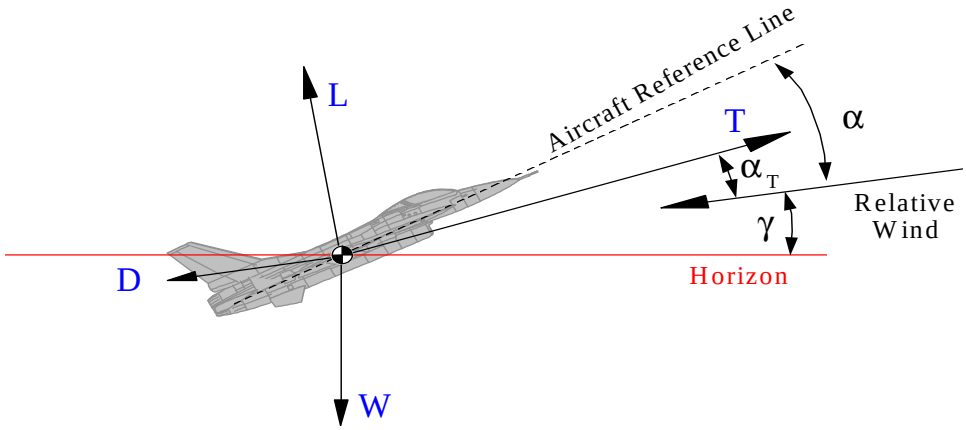

Figure 9.Forces on an Aircraft [26]

The flight path angle, γ, is the angle between the horizon and the aircraft's velocity vector (opposite the relative wind.) The angle of attack, α, is defined between the velocity vector and an aircraft reference line. The choice of the aircraft reference line is arbitrary. The designer is free to choose whatever reference is most convenient, provided care is taken to clearly specify this choice to all users of the aircraft performance data. The **thrust angle**, α_T, is the angle between the thrust vector and the velocity vector. This will not, in general, be the same as α, since the thrust vector will not generally be aligned with the aircraft reference line [26].

An important parameter which affects the lift, drag and thrust of an aircraft flying at relatively high velocities is the Mach number. Hence, the Mach number is defined, first.

a. Mach Number

At high speeds, considerable changes in the air density happen because the airflow around the airfoil of the wing suffers from the pressure changes. The changes in the air density then increases the effects of pressure that produce lift and pressure drag. The changes in the magnitudes in the lift and drag are called compressibility effects. Understanding compressibility effects is possible with Mach number. Mach number is the ratio of the flow velocity to the speed of sound. Free stream Mach number is the ratio of the speed of the aircraft to the speed of sound. Mach number is represented by the following equation:

$$\mathcal{M} = \frac{\mathcal{V}}{a} \tag{3}$$

where $\mathcal{M}$, $\mathcal{V}$, and a are the Mach number, velocity, and the speed of sound, respectively. The speed of sound at a specific altitude is derived by an equation provided in [27]

The Mach numbers are divided into five groups, called flight regimes in which the characteristics and effects of airflow differ. [26]:

$0.0 < \mathcal{M} < 0.3$ → Incompressible subsonic
$0.3 < \mathcal{M} < 0.8$ → Compressible subsonic
$0.8 < \mathcal{M} < 1.2$ → Transonic
$1.2 < \mathcal{M} < 5.0$ → Supersonic
$5.0 < \mathcal{M}$ → Hypersonic

Lower limit of the transonic regime, 0.8, is also called the critical Mach number. Because of the shape of the wing, the airflow over the upper surface of the airfoil is faster than the airflow. At Mach 0.8, the local Mach number on this surface of the airfoil may reach 1.0. So, this point is called the critical Mach number and all analyses beyond this point must consider the shock wave effects.

b. Thrust

Thrust is the force that drives the aircraft to move in the air. This force can be produced by turbo propellants, turbofans, turbojets, ramjets and rockets. Among the variety of alternatives, the most suitable one for the particular needs is chosen. Power of an aircraft engine is stated in a thrust to weight ratio. The engine power increases by the thrust it produces. Higher thrust provides the aircraft for higher velocity and lift. Most combat aircraft have 0.7-0.9 thrust to weight ratio. The F-15 and F-16 models have thrust to weight ratio more than 1.0; so, they can climb vertically [20].

The fighter aircraft which fly at subsonic, transonic and supersonic flight regimes are considered in this thesis. Propulsion for these flight regimes is provided by either turbofan or turbojet engines, and turbofan engines are discussed in this study.

(1) Turbofan Engines

This engine, as mentioned, is applied at subsonic, transonic and supersonic speeds. It drives both the compressor and a fan. The fan compresses both the main stream of air which is channeled through the engine and the supplementary stream which is ducted around the engine and discharged into the atmosphere. The main characteristic of the turbofan is that the thrust is greater than that of a turbojet with the same primary airflow capacity, and its fuel consumption is lower [23]. Once the gases have passed through the turbine, it is possible to mix more fuel with them and burn it to increase the exhaust velocity. The engine component which does this is called an afterburner [26]. Figure 10 illustrates a turbofan engine with afterburner.

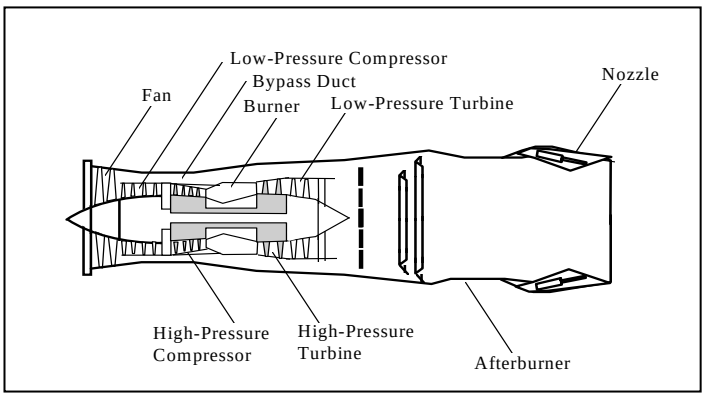

Figure 10.Turbofan with Afterburner [26]

The rate at which mass is flowing through a plane perpendicular to a one-dimensional flow is given by:

$$\dot{m} = \rho A V \tag{4}$$

where $\dot{m}$ is the mass flow rate, ρ is the air density at any altitude, A_C is the cross-sectional area of the stream tube, and V is the velocity. Consequently, the maximum available thrust force depends on two parameters in a specific aircraft. These are the altitude and the Mach number. Also, a pilot can change the throttle setting, u, to adjust the desired thrust. The maximum available thrust force produced by a turbofan engine is approximated by [26]

$$T_{max} = T_{SL} \left(\frac{\rho}{\rho_{SL}} \right) (1 + 0.7 M) \quad (5)$$

where subscript SL denotes the sea level. Air density values at various altitudes are calculated with a function [27] with respect to the International Civil Aviation Organization (ICAO) standard atmosphere.

In the light of these facts, the thrust force of an aircraft at a specific time can be represented by the following relationship:

$$T = u \, T_{max} (h , M) \quad (6)$$

c. Lift

Lift is generated by air moving across the surface of the wing. Due to the shape of the wing, movement of the air across the upper side of the wing is unbalanced to the bottom of the wing. As the curvature of the top of the wing is greater than the curvature of the bottom of the wing the air moves faster across the top of the wing. According to the principal discovered by Bernoulli, the faster gas travels, the lower its pressure. Consequently, because of the higher pressure on the bottom of the wing, the lift force that pushes up the wing is generated. The air flow on an airfoil is represented in Figure 11.

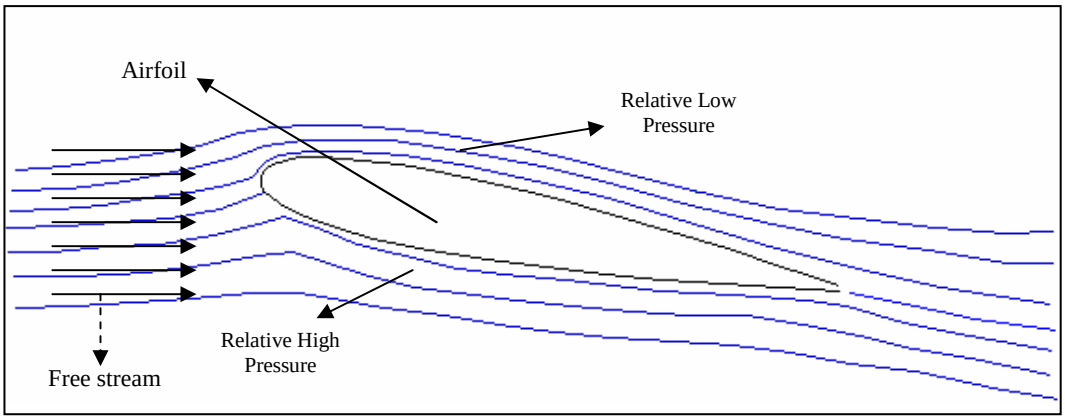

Figure 11.Air flow on an Airfoil.

The lift force of an aircraft is defined as

$$\mathcal{L} = C_{\mathcal{L}}\, q\, S \tag{7}$$

where $C_{\mathcal{L}}$ is a dimensionless coefficient which is called coefficient of lift, S is the reference area of the wing, and q is the free stream dynamic pressure which is represented by the equation

$$q = 0.5\, \rho\, \mathcal{V}^2 \tag{8}$$

Lift coefficient, $C_{\mathcal{L}}$, is the most important parameter to derive the lift. This coefficient defines the efficiency of the wing. Usually, lift of an airfoil is measured in wind tunnel tests. One of these tests with vast numbers of simulation results is conducted by NASA [29]

(1) Approximating the Lift Coefficient

Although the Eq. (7) seems simple and to give strong clues on the changes of the lift, there is always a problem to approximate the lift coefficient of the surfaces that produces lift. There are some simple and accurate theories to approximate the lift coefficient such as the thin airfoil theory and the lifting line theory.

There is one important point in this case is the angle of attack. Crucial changes on the lift coefficient occur while the angle of attack changes. Thus, before giving the details of the theories to approximate the lift coefficient, effects of angle of attack on the lift coefficient must be considered.

(a) Angle of Attack

Angle of attack of an aircraft is the angle between the velocity vector and the aircraft reference line, and affects the air flow around the airfoil. So, the lift coefficient has significant dependencies of angle of attack. Every surface of an aircraft has its own lift – angle of attack relationship. The total lift coefficient is the sum of all, and the overall lift coefficient – angle of attack will have similar

shape to that of a single airfoil. Figure 12 represents the typical lift – angle of attack curve.

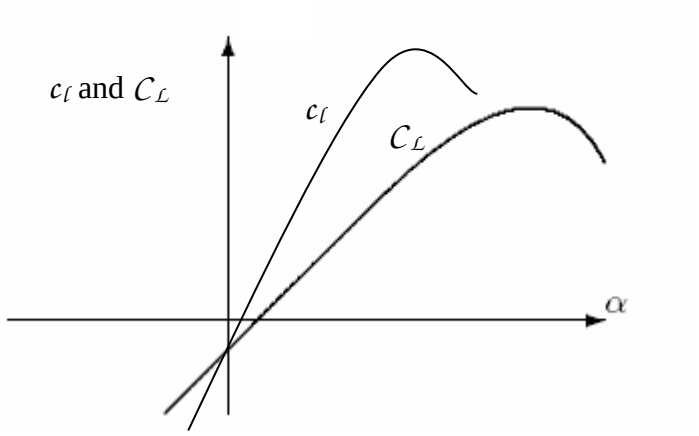

Figure 12.Lift vs. Angle of Attack Curve

Note that, for smaller angles of attack, the lift coefficient increases linearly. The rate of change of lift coefficient with angle of attack on this part of the curve is called the lift curve slope:

$$c_{l\alpha} = \frac{d\,c_l}{d\,\alpha} \qquad C_{L\alpha} = \frac{d\,C_L}{d\,\alpha} \tag{9}$$

The first term in the Eq. (9) is the two dimensional airfoil lift curve slope, and the second is the three dimensional finite wing lift curve slope.

At higher angles of attack, the air moving across the upper surface of the wing starts to separate from the wing and dissipates the lift. Gradually, the increase of the lift coefficient with angle of attack slows down and eventually reaches a maximum. More pressure drag is produced by the separation of airflow. This causes the drag coefficient to increase much more rapidly at higher angles of attack. After maximum lift coefficient is reached, additional increases in angle of attack causes less lift and the wings fail to carry the wings. This called stall, and the angle of attack for maximum lift coefficient is called the stall angle of attack, or α_{stall}.

(b) Thin Airfoil Theory

Thin Airfoil Theory is useful for approximating the lift coefficient and having an opinion about aerodynamic relationships. The equation for the Thin Airfoil Theory is

$$C_L = 2\pi\alpha \tag{10}$$

Though, it is not so useful, especially for engineers, because it pays no attention to the effects of the air flow over a wing. Particularly, this theory is ideal for approximating how the angle of attack affects the lift coefficient. Thus, it is an ideal approximation of the slope of the lift curve, $C_{L\alpha}$.

The lift coefficient curve is similar to the straight line algebraically, and can be represented by

$$C_L = C_{L\alpha}\alpha + C_{Lo} \tag{11}$$

where $C_{L\alpha}$, α, C_{Lo} are the slope of the lift curve, angle of attack and the zero-lift coefficient, respectively. According to the Thin Airfoil Theory, the slope of the lift curve, $C_{L\alpha}$, is equal to 2π, and the zero-lift coefficient, C_{Lo}, is equal to zero. Consequently, substituting these values in the Eq. (11) yields the form of the Thin Airfoil Theory which was stated in Eq. (10).

The problems with the Thin Airfoil Theory are [30]

- This theory assumes that the wing extends to infinity. In other words, the lifting surface has no wingtips. Wingtips introduce a form of drag called induced drag. The stronger the induced drag is, the lower the slope of the lift curve becomes.

- Thin Airfoil Theory doesn't account for the fact that the lift coefficient eventually reaches a maximum and then starts decreasing. According to Thin

Airfoil Theory, the lift coefficient increases at a constant rate, as the angle of attack increases, the lift coefficient increases.

(c) Lifting Line Theory

Lifting Line is another basic theory does provide a reasonable approximation for the lift coefficient and drag coefficient. This technique is called Prandtl's Lifting Line Theory [31]. Opposite to the Thin Airfoil Theory, the Lifting Line Theory applies to a finite wing with no sweep and a reasonably large aspect ratio. In simple terms, the wing is modeled as a fixed vortex with a series of trailing vortices extending behind it. These trailing vortices have the effect of reducing the lift produced by the wing and creating a form of drag called induced drag [31].

The lift coefficient according to the Lifting Line Theory is

$$C_L = c_{l\alpha} \left(\frac{\mathcal{AR}}{\mathcal{AR} + 2} \right) \alpha \tag{12}$$

where $c_{l\alpha}$ is 2D airfoil coefficient slope, $\mathcal{AR}$ is the aspect ratio which is equal to wingspan, b, squared, divided by the wing area, S, and α is the angle of attack. If the actual lift curve slope for the airfoil of the aircraft, $c_{l\alpha}$, is known, it can be used for that value. Otherwise, the approximate value for $c_{l\alpha}$ is 2π.

(d) Thin Airfoil Theory vs. Lifting Line Theory

In a test represented in [31], 2π is used for the slope of the lift curve, and the lift coefficients for two aircraft, Cessna 172 and Lightning, measured in wind tunnel are compared to both Thin Airfoil Theory and Lifting Line Theory. Figure 13 shows the results of the comparisons for Cessna 172 with a high aspect ratio, 7.37.

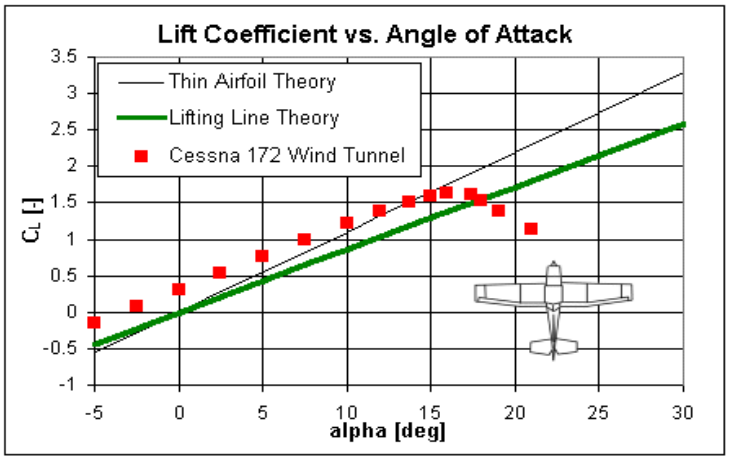

Figure 13.Lift Coefficient-Angle of Attack (Cessna 172) [31]

As it can be seen from Fig. 13 that, prediction made by Lifting Line Theory is slightly better than the one that made by the Thin Airfoil Theory when compared to the Cessna 172 wind tunnel data. Although the slope of the Lifting Line Theory matches the actual data better, neither this theory nor the Thin Airfoil Theory can predict stall angle of attack, and both provides a good estimate of the lift up to the stall angle.

The aircraft Lightning has an aspect ratio of 2.52, and has a swept wing. The Lifting Line Theory predicts the lift curve slope much better than the Thin Airfoil Theory does in the Lightning tests. Figure 14 represents the results for these tests.

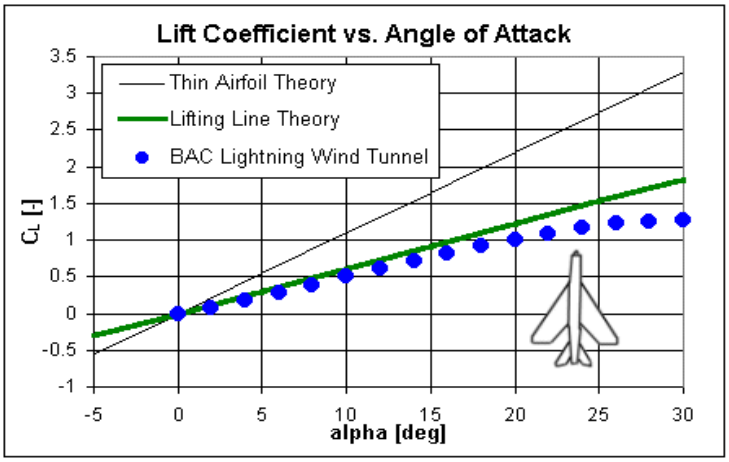

Figure 14.Lift Coefficient-Angle of Attack (Lightning) [31]

It must be noted that, even though the Lifting Line Theory assumes a wing with no sweep, it can produce nearly accurate approximation for the lift curve slope of the Lightning.

In both tests, the Lifting Line Theory has made better predictions for the slope of the lift curve than the Thin Airfoil Theory because of the consideration of the aspect ratio. By using this parameter, it becomes possible to estimate the effects of trailing vortices on the wing.

(e) Mach Number Effects on the Lift Coefficient

The features of the lift curves of fighter aircraft will vary with Mach number. The most important effect of Mach number is the changes in the slope of the lift coefficient curves, $C_{L\alpha}$. Hence, some corrections must be applied to these curves to account for the compressibility affects. Practical correction method applied to the lift curve slopes in the subsonic regime is the Prandtl-Glauert correction:

$$c_{l\alpha} = \frac{c_{l\alpha(M=0)}}{\sqrt{1-M^2}} \tag{13}$$

In the subsonic regime, the relation between the slope of two dimensional airfoil lift curve, $c_{l\alpha}$, and that of the three dimensional wing lift curve, $C_{L\alpha}$, doesn't change so much. So, the same correction may be applied to $C_{L\alpha}$.

$$C_{L\alpha} = \frac{C_{L\alpha\,(M=0)}}{\sqrt{1-M^2}} \tag{14}$$

Equations (13), (14) are valid and useful in subsonic regime only. In the wake of compressibility, it's not necessary to make corrections where $M < 0.3$.

At supersonic speeds, the lift curve slope is

$$c_{L\alpha} = \frac{4}{\sqrt{M^2 - 1}} \tag{15}$$

d. Drag

Drag is basically the resistance of the air against an aircraft, and acts against the thrust of the aircraft. To maintain the current velocity, for a steady level flight, the thrust which is at least equivalent of the drag must be provided. Every surface of an aircraft causes drag. The overall drag is separated into components whose significance is associated with either the physical nature of the flow field or the geometry of the body [28].

The most common decomposition of drag consists of dividing the overall drag into the zero-lift drag and the induced drag. The induced drag contains any kind of drag produced by the lift. So, the overall drag can be defined in coefficient form as

$$C_D = C_{D0} + C_{Di} \tag{16}$$

where C_{D0} is zero-lift drag coefficient, and C_{Di} is the induced drag coefficient. The zero lift drag includes both friction drag and the pressure drag which is caused by vortices, flow separation (as mentioned in the preceding section), or formation of shock wave in the supersonic regime.

(1) Lift-to-Drag Ratio

Lift-to-drag ratio is an important parameter for an aircraft. Another name of this parameter is aerodynamic efficiency

$$E = \frac{L}{D} = \frac{C_L}{C_D} \tag{17}$$

and depends on the Mach number and the angle of attack. Representative values of E_{max} are 10-25 for subsonic aircraft, and 5-10 for supersonic aircraft [28].

(2) Parabolic Drag Polar

Drag polar is the variation of an aircraft's drag coefficient with its lift coefficient [26]. This in an important value, so that maximum speed, rate and of climb, range, and endurance depends on the drag polar. Any kinds of drag can be approximated by the Eq. (16) where

$$C_{Di} = k_1 C^2_L + k_2 C_L \tag{18}$$

Then, the total drag coefficient becomes

$$C_D = C_{Do} + k_1 C^2_L + k_2 C_L \tag{19}$$

In Eqs. (18) and (19) k_1 denotes an aircraft-specific constant characteristic, and can be expressed by

$$k_1 = \frac{1}{\pi e_o AR} \tag{20}$$

for subsonic speeds. k_1 can be approximated by the following equation for supersonic speeds:

$$k_1 = \frac{AR\,(M^2 - 1)}{(4\,AR\sqrt{M^2 - 1}) - 2} \cos \Lambda_{LE} \tag{21}$$

where Λ_{LE} is the sweep angle on the leading edge of the wing. The symbol AR denotes the aspect ratio which is equal to wingspan, b, squared, divided by the wing area, S. It's obvious from Eqs. (19), (20) and (21) that induced drag is inversely proportional to the aspect ratio. This implies that a wing with low aspect ratio causes high induced drag. The other variable in Eq. (20) is the Oswald's

efficiency factor, e_o, which accounts for the non-ellipticity of the lift distribution over the wing, the increase in the skin friction drag of the wing angle of attack, and the increase in the fuselage drag with angle of attack [28]. Generally, Oswald's efficiency factor is between 0.6-0.9. In this study, this factor is calculated by the equation obtained with a curve fit of wind tunnel data for a variety of wing and wing-body combinations. [26]

$$e_o = 4.61\,(1-0.045\,\mathcal{AR}^{0.68})\,(\cos \Lambda_{LE})^{0.15} - 3.1 \qquad (22)$$

The effects of k_2 in subsonic and supersonic flight regimes are negligible, but at speeds exceeding critical mach number, this value must be taken into account.

The zero-lift drag of a subsonic aircraft is composed of friction drag and pressure drag. Flow separation causes the pressure drag. The relative importance of the pressure drag with respect to the friction drag depends on the thickness ratio, the ratio of the maximum thickness to the chord for a wing. Since the thickness ratio for a wing unusually exceeds 0.2, pressure drag can be neglected [28]. Also, the parasitic effects are generally small in the subsonic region, a method called the wetted area can be used to estimate the zero-lift drag coefficient. According to this method, a uniform skin friction coefficient can be assumed for the different surfaces of the aircraft. Thus, the zero-lift drag coefficient becomes

$$C_{Do} = C_f \frac{\mathcal{S}_{wet}}{\mathcal{S}} \qquad (23)$$

where $\mathcal{S}_{wet}$ is the wetted area, that is, all the surface area over which air flows, and $\mathcal{S}$ is the reference wing surface. Finally, C_f is the skin friction coefficient, and typically 0.035 is used for a fighter aircraft [26].

For the supersonic flight regime, wave drag, which is assumed constant in this thesis, is added to the zero lift-drag which is used as a tabular data in this work. Thus the zero lift drag becomes

$$C_{D_o} = C_f \frac{S_{wet}}{S} + C_{D_{wave}} \tag{24}$$

Consequently, total drag is calculated by the following equation:

$$D = C_D \, q \, S \tag{25}$$

where, q is dynamic pressure as defined in Eq.(8), and S is the reference area.

e. Weight

Weight is the force opposite to lift. It is the effect of gravitational acceleration on the aircraft, and is defined as

$$W = m \, g \tag{26}$$

where m is the total mass of the aircraft, and g is the acceleration of gravity which is equal to 9.81 m/sec^2.

2. Equations of Motion over a Flat Earth

As this study is concerned with scenarios that occur in short ranges, the earth is regarded as flat and non-rotating. The general simplified equation for flight can be represented by [28]

$$T + A + mg = ma = m \frac{dV}{dt} \tag{27}$$

where T is the thrust, A the aerodynamic force, m the mass, g is the acceleration of gravity, a the acceleration of the aircraft with respect to the Earth.

The velocity of the aircraft with respect to the Earth is denoted by the equation

$$\mathcal{V} = \frac{d\mathcal{E}O}{dt} \tag{28}$$

where $\mathcal{E}O$ is the vector that connects a point on the Earth with the aircraft.

a. Coordinate Systems of Interest

The coordinate systems for flight over a flat earth are

- the ground axes system,
- the local horizon system,
- the wind axes system,
- the body axes system.

These axes systems are defined with the assumption that aircraft has a plane of symmetry. Plane of symmetry is the flat plane that splits the aircraft into right and left halves.

Note that, the coordinate systems described below are all right handed and orthogonal.

(1) The Ground Axes System

- This coordinate system has its origin, point E, fixed to an arbitrary point on the surface of the Earth (Fig.15),

- The z-axis is vertical, points downward and positive downward,

- The x-axis and the y-axis are contained in a horizontal plane,

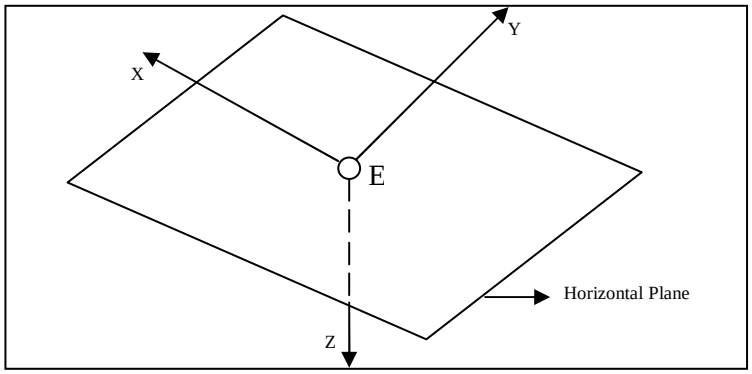

Figure 15.The Ground Axes System

(2) The Local Horizon System

- This coordinate system has its origin on an arbitrary point that may move relative to the Earth (see Fig.16). For example, the origin may be fixed to the center of gravity (CG) of an aircraft and move with the CG [28].

- The axes orientations are identical with the axes in the ground axes system.

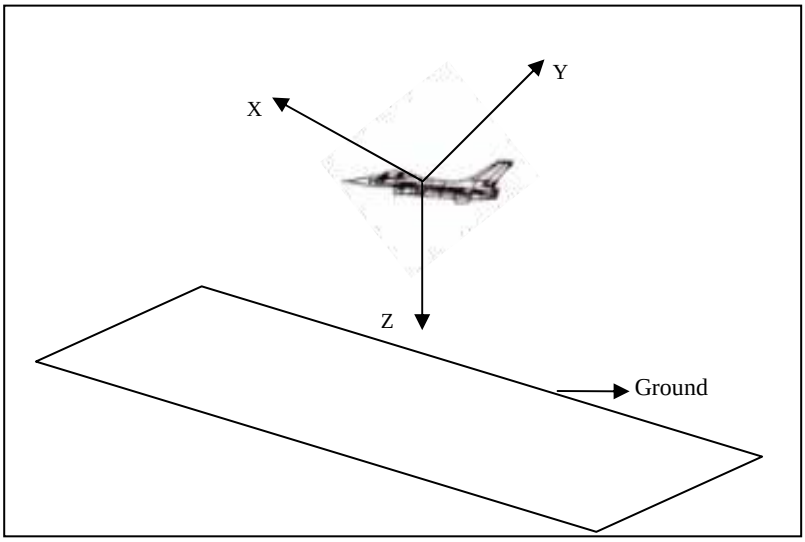

Figure 16.The Local Horizon System

(3) The Wind Axes System

- The atmosphere is assumed to be at rest with respect to the Earth,

- The x-axis is tangent to the flight path and positive forward,

- The z-axis is perpendicular to the x-axis, positive downward and in the plane of symmetry,

- The y-axis is to the right of the plane of symmetry.

The wind axes system is represented in Figure 17.

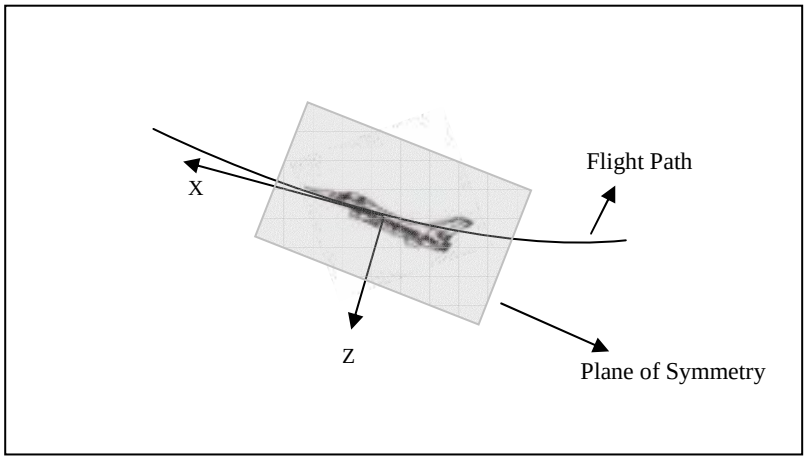

Figure 17.The Wind Axes System

(4) The Body Axes System

- The x-axis is contained in the plane of symmetry and positive forward,

- The z-axis is perpendicular to the x-axis in the plane of symmetry and positive downward,

- The y-axis is perpendicular to the plane of symmetry. (See Fig. 18)

Figure 18.The Body Axes System [32]

b. Angular Relationship between Wind Axes – Local Horizon

The position of the aircraft relative to the Earth can be found by representing the velocity in the local horizon. To do so, the needed orientation of the wind axes with respect to the local horizon is described in terms of three angular parameters. Conventionally, the transformations are based on three rotations of the heading angle or velocity yaw, χ, flight path angle or velocity pitch, γ, and the bank angle or velocity roll, μ. The transformations can be represented by the matrix equations. First, the local horizon is rotated by χ around the z-axis.

$$\begin{pmatrix} i_1 \\ j_1 \\ k_1 \end{pmatrix} = \begin{pmatrix} \cos\chi & \sin\chi & 0 \\ -\sin\chi & \cos\chi & 0 \\ 0 & 0 & 1 \end{pmatrix} \begin{pmatrix} i_h \\ j_h \\ k_h \end{pmatrix} \tag{29}$$

The obtained system is rotated by γ around the new y-axis

$$\begin{pmatrix} i_2 \\ j_2 \\ k_2 \end{pmatrix} = \begin{pmatrix} \cos\gamma & 0 & -\sin\gamma \\ 0 & 1 & 0 \\ \sin\gamma & 0 & \cos\gamma \end{pmatrix} \begin{pmatrix} i_1 \\ j_1 \\ k_1 \end{pmatrix} \tag{30}$$

Lastly, the wind axes system is obtained from the system represented in Eq. (30) by means of a rotation μ around the x-axis.

$$\begin{pmatrix} i_w \\ j_w \\ k_w \end{pmatrix} = \begin{pmatrix} 1 & 0 & 0 \\ 0 & \cos\mu & \sin\mu \\ 0 & -\sin\mu & \cos\mu \end{pmatrix} \begin{pmatrix} i_2 \\ j_2 \\ k_2 \end{pmatrix} \tag{31}$$

Consequently, the relationship between the wind axes and the local horizon is obtained by performing a matrix multiplication as seen below.

$$\begin{pmatrix} i_w \\ j_w \\ k_w \end{pmatrix} = \begin{pmatrix} \cos\gamma\cos\chi & \cos\gamma\sin\chi & -\sin\gamma \\ \sin\mu\sin\gamma\cos\chi - \cos\mu\sin\chi & \sin\mu\sin\gamma\sin\chi + \cos\mu\cos\chi & \sin\mu\cos\gamma \\ \cos\mu\sin\gamma\cos\chi + \sin\mu\sin\chi & \cos\mu\sin\gamma\sin\chi - \sin\mu\cos\chi & \cos\mu\cos\gamma \end{pmatrix} \begin{pmatrix} i_h \\ j_h \\ k_h \end{pmatrix} \tag{32}$$

c. Derivation of Kinematic Equations

The velocity of an aircraft is parallel with the x_w-axis. Since, the velocity, $\mathcal{V}$, in Eq. (28) can be represented by [28]

$$\mathcal{V} = \mathrm{V} i_w = \mathrm{V} \left[\cos \Upsilon \cos \chi \, i_h + \cos \Upsilon \sin \chi \, j_h - \sin \Upsilon \, k_h \right] \tag{33}$$

The vector that connects the point on the Earth with the aircraft, $\mathcal{EO}$, can be written in the form,

$$\mathcal{EO} = \mathrm{X} \, i_h + \mathrm{Y} \, j_h + \mathrm{Z} k_h \tag{34}$$

and its time derivative is

$$\frac{d\mathcal{EO}}{dt} = \dot{\mathrm{X}} \, i_h + \dot{\mathrm{Y}} \, j_h - \dot{h} \, k_h \tag{35}$$

In Eq. (35), the altitude above sea level satisfies the following

$$h = -\mathrm{Z} + const \tag{36}$$

As a consequence, the kinematic equations of motion are obtained by combining the Eqs. (28), (33), and (35):

$$\dot{\mathrm{X}} = \mathrm{V} \cos \Upsilon \cos \chi \tag{37}$$

$$\dot{\mathrm{Y}} = \mathrm{V} \cos \Upsilon \sin \chi \tag{38}$$

$$\dot{h} = \mathrm{V} \sin \Upsilon \tag{39}$$

d. Equations of Motion for Specific Flight Paths

The three dimensional point mass model including aerodynamic forces are used for the aircraft. Figure 19 represents the symbolic definitions for this

model. The control variables in the model are the angle of attack for rotations around the y-axis, the bank angle for rotations around the x-axis, and the throttle setting that is the proportion of the available thrust used.

The detailed information about the equations of motion and turn performance of an aircraft can be found in [23, 26, 28, 33].

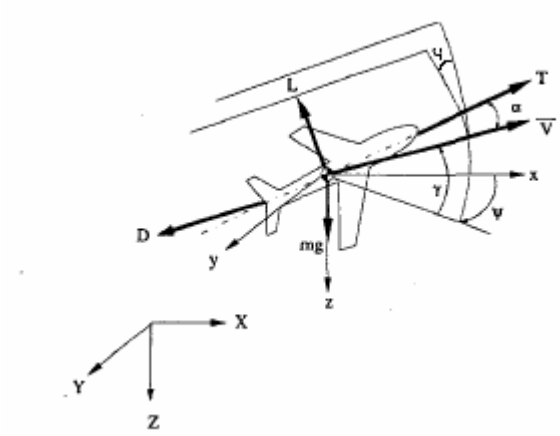

Figure 19. 3D Aircraft Model [5]

(1) Equations of Motion in the Vertical Plane

In this section, kinematic relationships in the vertical plane are discussed. Flight in the vertical plane implies that there is no positional change in the y-axis, and it leads the heading angle, χ, to be zero. In this condition, the control variable, i.e. bank angle, μ, needed to change the heading angle is also zero. Thus, the plane of symmetry is vertical plane, and motion of a fighter is represented by the following equations:

$$\dot{X} = V \cos\gamma \tag{40}$$

$$\dot{h} = V \sin\gamma \tag{41}$$

$$\dot{\gamma} = \frac{L + u_T \sin\alpha}{m v} - \frac{g \cos\gamma}{v} \tag{42}$$

$$\dot{v} = \frac{u_T \cos\alpha - D}{m} - g \sin\gamma \tag{43}$$

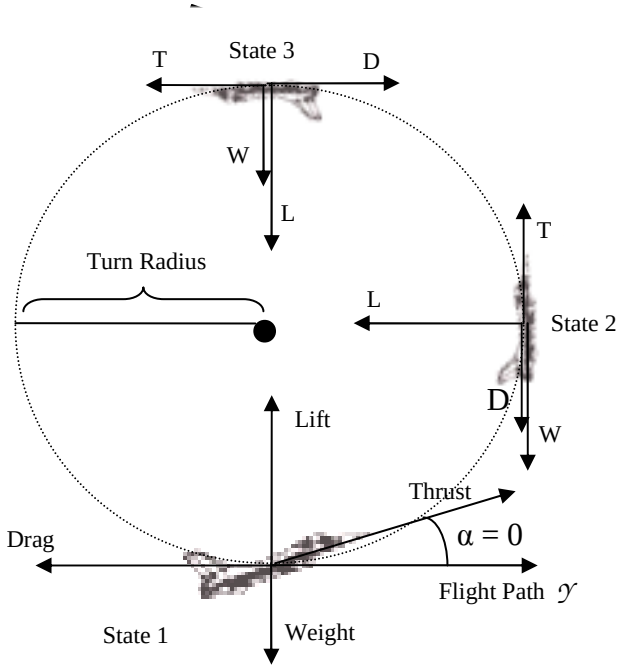

Figure 20.Forces for a Turn in a Vertical Plane

Note that, in Figure 20, the angle of attack, α, is zero and exaggerated for the sake of generalization.

A vertical maneuver in which 360 degrees of turn is performed is called a loop. The state 1 in Figure 20 represents the initial conditions of the loop. The action performed at this state is called a “pull up”. At state 2, is vertical to the ground. At the top of the loop, the fighter performs a “pull-down”. The conditions at this state are represented by state 3. A pull-down may also be the initial state of the loop if a fighter in a straight and level flight performs a 180-degree roll by changing the bank angle, μ. If a vertical turn maneuver is performed by rolling 180^{o} first, and then pulling down until the flight path is inverted, this is the special maneuver known as the split-s.

As discussed in the previous chapter, the parameters of great importance for fighter performance are the turn radius and the turn rate. These parameters are calculated by summing the forces perpendicular to the velocity vector (the flight path).

For the state 1 in Figure 20 (pull up):

$$F = m\,a = m\,\frac{V^2}{r} = \frac{W\,V^2}{g\,r} = L - W \tag{44}$$

$$\frac{V^2}{r} = \frac{L}{W} - 1 = n - 1 \tag{45}$$

$$r = \frac{V^2}{g\,(n - 1)} \tag{46}$$

$$w = \frac{g\,(n - 1)}{V^2} \tag{47}$$

For the state 2 (vertical velocity vector):

$$F = L \tag{48}$$

$$r = \frac{V^2}{g\,n} \tag{49}$$

$$w = \frac{g\,n}{V} \tag{50}$$

For the state 3 (pull down), the parameters are

$$F = L + W \tag{51}$$

$$r = \frac{V^2}{g\,(n + 1)} \tag{52}$$

$$w = \frac{g\,(n + 1)}{V} \tag{53}$$

(2) Equations of Motion in the Horizontal Plane

This section considers the kinematic and dynamic relationships in the horizontal plane. Flight in the horizontal plane implies that there is no positional change in the z-axis, and it leads the flight path angle, γ, to be zero (see Fig. 21). Consequently, equations of motion of a fighter in the horizontal plane is represented by

$$\dot{X} = V \cos \chi \tag{54}$$

$$\dot{Y} = V \sin \chi \tag{55}$$

$$\dot{\chi} = \frac{(L + u T \sin\alpha) \sin \mu}{m v} \tag{56}$$

$$\dot{v} = \frac{u T \cos\alpha - D}{m} \tag{57}$$

In a horizontal turn, the fighter maintains its altitude, thus, the directions of the velocity vector of the aircraft changes but stands in the vertical plane. It means that the vertical opponent of the lift force is equal to the weight. So, the load factor, n, the g's that the fighter is pulling, becomes

$$L \cos \mu = W \tag{58}$$

$$n = 1 / \cos \mu = L / W \tag{59}$$

and the important parameters for fighter performance, the turn radius and the turn rate, are

$$r = \frac{V^2}{g \sqrt{n^2 - 1}} \tag{60}$$

$$w = \frac{g \sqrt{n^2 - 1}}{V} \tag{61}$$

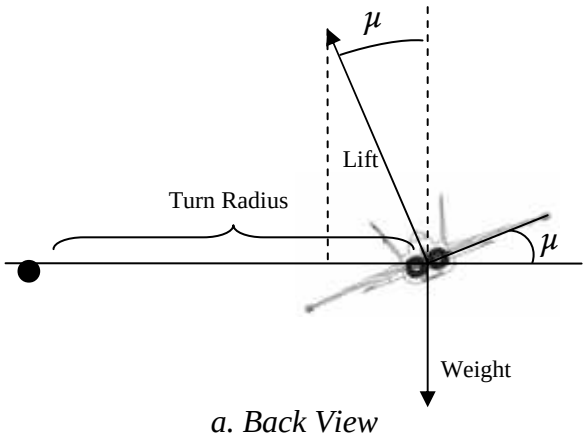

a. Back View

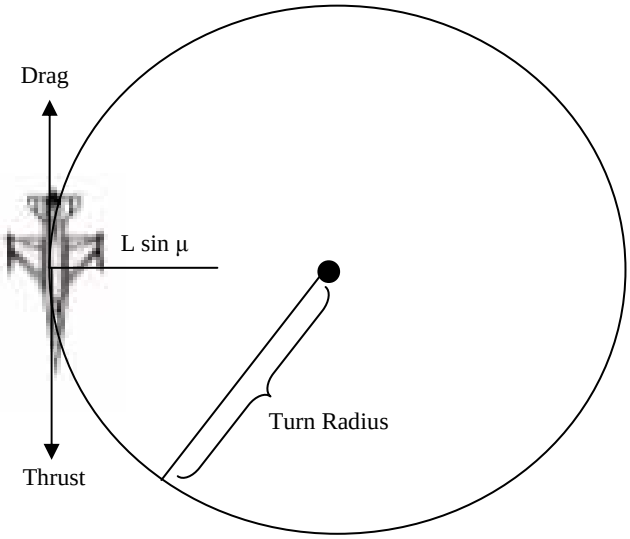

b. Top View

Figure 21.Forces for a Turn in a Horizontal Plane

One more point for a flight in a horizontal plane is the magnitude of the velocity vector. The magnitude of the velocity vector is calculated by summing the forces parallel to the fighter's velocity vector.

$$F_v = m\,a = \frac{W}{g}\,\frac{dV}{dt} = T - D \qquad (62)$$

For a free maneuvering flight, a fighter may perform sustained turns. In these types of turns, the fighter maintains the same turn rate and the turn radius for a long time. So, for sustained turns in the horizontal plane, the magnitude of the velocity vector doesn't change. This yields that

$$T = D \qquad (63)$$

but, under missile threat, instantaneous turns must be performed. This requires instantaneous changes in the velocity vector. Consequently, the thrust is usually not equal to the drag in instantaneous turns.

(3) General Equations of Motion

The flight paths discussed above are only two of available to a fighter pilot. In the vertical plane, the control variable, i.e. bank angle, to make a fighter roll is assumed to be zero. In the horizontal plane, it's assumed that the flight path angle of the fighter is zero which implies that there is no change in the altitude. But, in the real life, a fighter pilot performs infinite number of maneuvers including directional changes in both the vertical and the horizontal planes. All other maneuver planes are called "oblique turns" [23]. The equations of motion for oblique turns can be derived by combining the equations of motion in the vertical plane and the horizontal frame. Consequently, the general equations of motion are as follows:

$$\dot{X} = V \cos\gamma \cos\chi \tag{64}$$

$$\dot{Y} = V \cos\gamma \sin\chi \tag{65}$$

$$\dot{h} = V \sin\gamma \tag{66}$$

$$\dot{\gamma} = \frac{(L + u T \sin\alpha)\cos\mu}{m v} - \frac{g \cos\gamma}{v} \tag{67}$$

$$\dot{\chi} = \frac{(L + u T \sin\alpha)\sin\mu}{m v} \tag{68}$$

$$\dot{v} = \frac{u T \cos\alpha - D}{m} - g \sin\gamma \tag{69}$$

X, Y, h, γ, χ, and v are X and Y the range, the altitude, the flight path angle, the heading angle, and the velocity, respectively. g is the acceleration of gravity, m is the mass of the aircraft. T, L, D denote the maximum available thrust of the aircraft, the lift and the parabolic drag polar respectively. The control variables are the angle of attack α, the throttle setting u, and the bank angle μ.

3. Missile Model

The missile's guidance system is the Proportional Navigation. Theoretically, this law issues acceleration commands, perpendicular to the instantaneous missile-aircraft line-of-sight, which are proportional to the line-of-sight rate and closing velocity [1]. The guidance law can be stated as

$$n_c = \mathcal{N}' V_c \dot{\lambda} \tag{70}$$

where n_c is the acceleration command, $\mathcal{N}'$ a unitless gain (usually in range of 3-5) known as the effective navigation ratio, and λ the line-of-sight rate.

The equations of motion of a missile are In this study, the proposed implementation of proportional navigation guidance law in [2], and [4] is used as the pursuing missile's guidance system.

III. VISUAL END-GAME SIMULATION (VEGAS)

The VEGAS software that is developed to analyze the performance of the aircraft and the missile is implemented with Visual C++ (R) 6.0. OpenGL library functions are used for visualization. Simulations are run on an IBM laptop with Pentium (R) CPU 2.60 GHz processor and 512 Mbs of RAM. The operating system on the computer is Microsoft Windows XP.

A. INTRODUCTION

The terminal phase of a missile-aircraft encounter is also called an end-game. The avoidance problem of a fighter can be divided into two parts [11]; the missile outrunning and the end-game. The missile outrunning is caused by the finite burn time of a missile rocket and subsequent rapid energy dissipation by the aerodynamic drag. With suitable maneuvers, the relative velocity between the missile and the fighter (i.e., closing velocity) may be reduced to zero before the interception. If this is not achieved, the end game begins.

One of the aims of this study is to explore the attitudes of the fighter in the latest phase of the encounter. Hence, first, the fighter evasive maneuvers against missiles are investigated. It is realized that, there are some basic maneuvers that constitute the evasive maneuvers in an air combat. Besides, It is also noticed that the corner speed, turn rate, turn radius must be taken into account. These facts have leaded us to examine the aerodynamic forces and orientation kinematics which directly affects the motion of the aircraft and this topics have been studied in detail.

Simultaneously, Moran [2] has searched the guidance methods of missiles, especially the proportional navigation which is the most widely used guidance method for the guided missiles with active homing capability.

To evaluate the motions of a fighter aircraft and the fighter evasive maneuvers against proportional navigation, a new software program called Visual

End-Game Simulation (VEGAS) has been developed. All the factors mentioned above are included in this software. Extensive simulation results that are supported by comprehensible visual projections have been gathered.

Visual C++ and Open GL are used in simulations. OpenGL's main purpose is to render two and three-dimensional objects into a frame buffer [34]. A 3D visualization is performed in order to provide the user for a comprehensive understanding about the terminal phase of the encounter.

The structure of the software is detailed in the next section.

B. STRUCTURE OF VEGAS

Five modules constitute the VEGAS. These are

- Main,
- Evader,
- Pursuer,
- Radar,
- Aero

modules. Figure 22 represents the structure of the VEGAS.

The main module of the VEGAS serves as the manager of the simulation which initializes the simulation, calls the pursuer module and the evader module and handles visual projections.

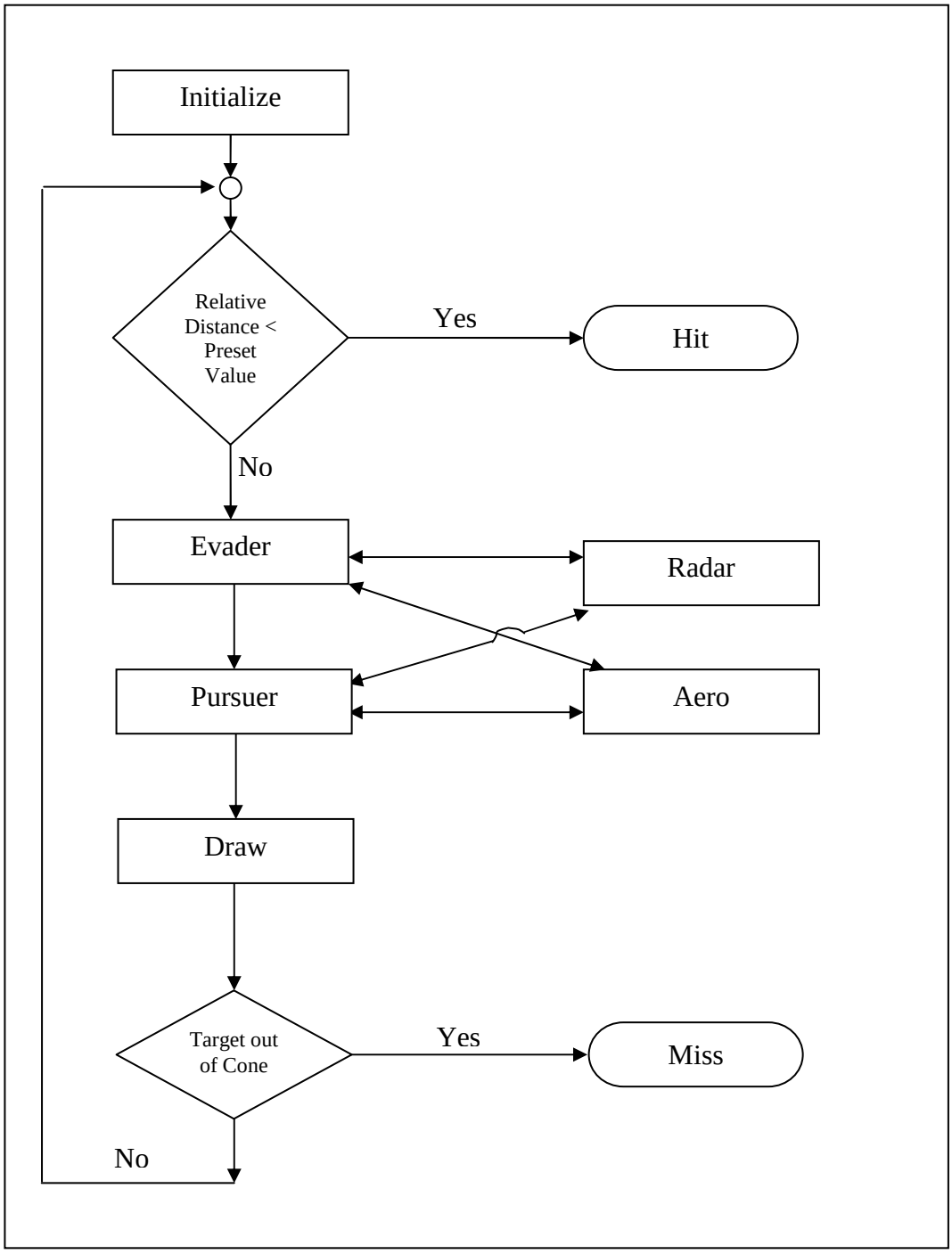

Figure 22.Structure of Visual End-Game Simulation (VEGAS)

The “pursuer” module is the program of missile’s seeker model and maneuvers. A missile pursuing an aircraft with proportional navigation guidance is taken into consideration. The missile seeker implementation is detailed in [2] and [4].

The current coordinates of the missile and the target is provided for the pursuer and evader modules by the “radar” module.

The required values for aerodynamic calculations, the air density and the Mach numbers equivalent to the vehicle velocities are computed in the “aero” module.

The “evader” module is the main subject of this thesis. In this part of the simulation program, a generic aircraft with high-g capability and its maneuvers are modeled.

A detailed explanation of each module is given in the following sections.

1. Main Module

Main module is the manager of the simulation, as defined above, which initializes the simulation, calls the functions of pursuer’s and evader’s maneuvers and handles visual projections.

At the beginning of the program, the visual settings are initiated by the OpenGL functions. The position of the camera and the point where the camera will be oriented are adjusted. These settings are organized so that any viewport alternatives can be chosen according to the user’s preference. That is to say, the camera can be either moving or fixed. Some of the camera position and orientation alternatives are

- from a fixed point to the position of either the fighter or the missile,
- from a fixed point so that the user can view both vehicles,
- from the position of the missile to that of the fighter, vice versa,
- from a point which is close to one of the vehicles to the position of that vehicle, thus, the user can view and visually analyze the motions of that vehicle.

In the main module, the initial values of the missile-fighter encounter state are provided for the simulation. The user of the VEGAS can enter these values manually, so he has the initiative to choose the desired maneuver. The initial states of the encounter for both vehicles are

- x, y, z positions relative to the origin,
- velocities of the vehicles,
- reference areas (i.e. wing, fuselage),
- maximum thrust force,
- the flight path angle,
- the heading angle.

Also, the user of VEGAS can choose the evasive maneuver which he wants the fighter to perform via a menu.

The simulation is divided into fixed time steps. At each time step, the maneuvers of the vehicles are performed, and the new state variables are stored in a predefined variable for the subsequent time step.

After the initialization, the evader and the pursuer modules are called respectively. In each module, the recent states of the vehicles are stored in arrays. When the pursuer returns, the changed data of both vehicles stored in the arrays are evaluated, and the vehicles are drawn on the screen.

Before running the next step, the relative distance between the missile and the fighter is compared with the terminal condition, i.e. the predefined relative distance between the vehicles. The next step is run unless the terminal condition is reached. When the terminal condition is reached, the simulation ends. At this point, the trajectory histories for both of the vehicles can be viewed in three-dimensions at any camera position. The position of the camera is changed by the

keyboard commands. This feature helps the user to clearly observe the attitudes of the missile and the fighter throughout the encounter scenario.

2. Pursuer Module

As mentioned before, the guidance system of the missile is the proportional navigation. According to the proportional navigation, the missile estimates the respective motion and the position of the fighter and is oriented towards that point. The attitudes of the missile to intercept the fighter aircraft according to this guidance system including realistic aerodynamics are implemented in this module. This module is designed by Moran, I. [2]

3. Radar Module

The radar module supplies the vehicles with the latest three-dimensional coordinates of the adversary. This module is called by both of the vehicles. Figure 23 represents the flow chart of the radar module.

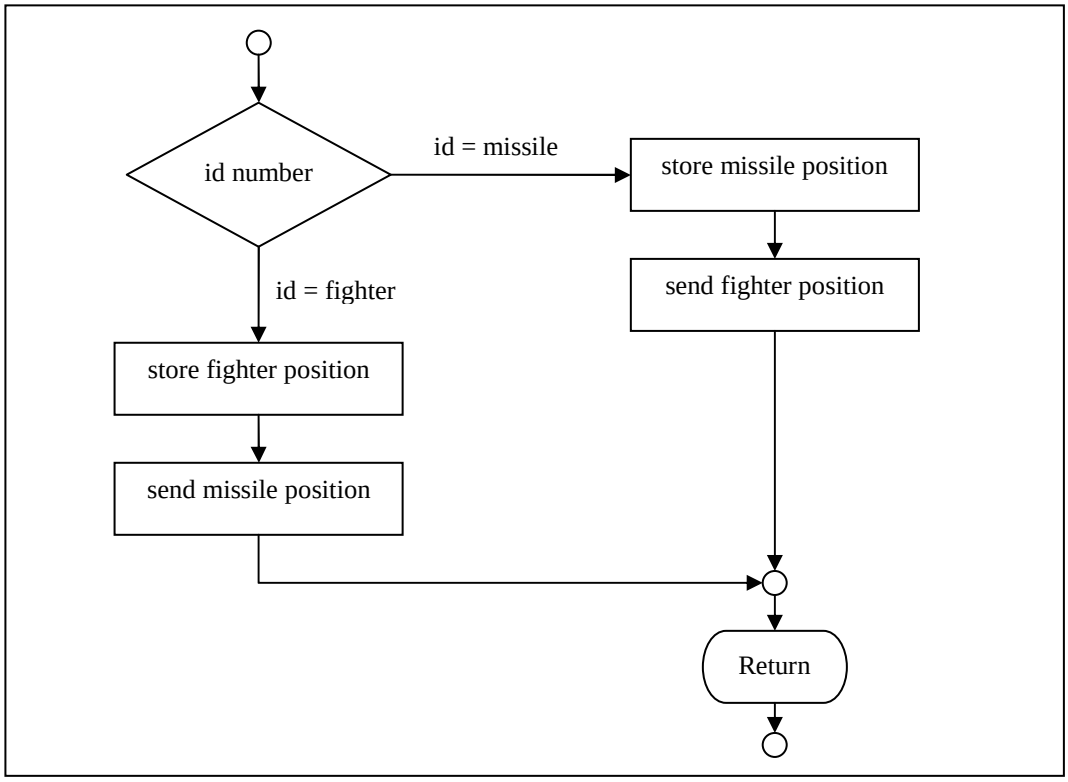

Figure 23. Flow Chart of the Radar Module.

When the evader finishes it recent motion, it passes its id number and its latest x, y, and z coordinates to the radar module. When the radar module receives this data, it decides whose data is received with respect of the id number. As this data in our example is of the evader, the radar module stores the coordinates of the evader in a structural variable, and sends the coordinates of the missile to the evader module.

Consequently, in this case, this module acts as the radar of the fighter. In the other hand, when the pursuer module calls this module, it acts as the seeker radar of the missile.

The limitations, such as radar range, observation cone, of both vehicles can be added to the radar module because of its modular structure. So, it is apt to any kind of realistic development, and this is a strong advantage of the VEGAS.

4. Aero Module

In the aero module, two values needed by the vehicles for aerodynamic calculations are computed. These are

- The air density at the altitude of the calling vehicle module,
- The Mach number in respect of the altitude and the velocity of the calling vehicle.

The air density at a specific altitude, and the speed of sound, which is needed for deriving the equivalent Mach number values regarding the velocities of the vehicles are computed by the equations provided in [27].

5. Evader Module

The evader module is the part of VEGAS where the evasive maneuvers of the fighter are implemented. The fighter aircraft modeled herein is an extended point mass model including orientation kinematics and aerodynamics. According to this model

- The Earth is assumed to be flat,
- The side-slip angle is assumed to be zero.

and, the fighter

- moves in a three-dimensional scenario space,
- performs bank-to-turn maneuvers in order to change direction,
- is dependent of aerodynamic forces,
- changes its flight path angle by applying angle of attack, α, commands,
- changes its heading angle by applying bank angle, μ, commands, and
- applies desired thrust force by adjusting throttle setting, u, where $0<u<1$.

When the evader module is called by the evermain module at the first time step, the initial states are assigned into local state variables. Then, the selected evasive maneuver is performed starting at these initial states.

In order to compute the motion of aircraft at each time step, an array of aerodynamic calculations is made. These aerodynamic calculations include deriving the followings:

- Mach number by calling the aero module,
- lift curve slope regarding the Mach number,
- lift coefficient and lift force,
- zero-lift drag coefficient, total drag coefficient and total drag force,
- pitch rate, which has an aircraft-specific maximum value,

- change in the flight path angle, and the new flight path angle,

- change in the heading angle, and the new heading angle,

- acceleration and the new velocity,

- load factor,

- the turn radius an the turn rate values for analyzing the performance of the fighter.

After the aerodynamic calculations are made, the selected maneuver is performed, the latest state and control variables are written into an output file, the radar module is called in order to send the latest coordinates and to receive the coordinates of the missile.

In order to the fighter maneuvers to be realistic, some aircraft-specific limitations, such as the load factor, pitch rate, roll rate, max.-min. operation altitudes, are considered. The maneuvers are implemented so that the aircraft always performs its maneuvers without exceeding the specified limitations. Also every basic fighter maneuvers are designed as separate sub-functions. This makes it possible to analyze different maneuver combinations, also, makes the simulation apt to further maneuver attachments.

IV. PERFORMANCE EVALUATION

The performance evaluation of the fighter aircraft and its evasive maneuvers are made by using the Visual End-Game Simulation (VEGAS) software developed in the Naval Science and Engineering Institute.

A. NUMERICAL ANAYSIS

1. Aircraft Characteristics

The aircraft data used in the simulations represents a generic supersonic fighter with high-g capability. The parameters of the fighter modeled in this study are tabulated in Table 1.

Table 1.Aircraft Characteristics [26, 35, 36]

Mass, m	13607.7711 kg
Thrust at Sea Level, T_{SL}	77.84 kN
Wetted Area, S_{wet}	138.89 m^2
Wing Area, S	27.870912 m^2
Aspect Ratio, AR	4.08
Wing Sweep Angle, Λ_{LE}	40^o
Maximum Speed, V_{max}	603 m/sec
Maximum Load Factor, n_{max}	9 g
Skin Friction Coefficient, C_f	0.0035
Wave Drag Coefficient	0.0261
Lift Curve Slope at M=0, $c_{l\alpha(M=0)}$	5.73 / ^{o}
Min. /Max. Usable Angle of Attack, α	-2^o / $+25^o$

2. Aerodynamic Calculations

a. Maximum Available Thrust

In this section, the aerodynamic calculations for the fighter whose characteristics are tabulated in Table 1 are examined. Firstly, the available thrust force variation according to the Mach number is shown. As it was mentioned in the chapter 2, the thrust force is a function of the altitude and the Mach number at which an aircraft is flying. As the Mach number increases, the available thrust that an engine produces decreases. The thrust variation of the fighter model according to the Mach number is approximated by the Eq. (5) and is represented in Figure 24.

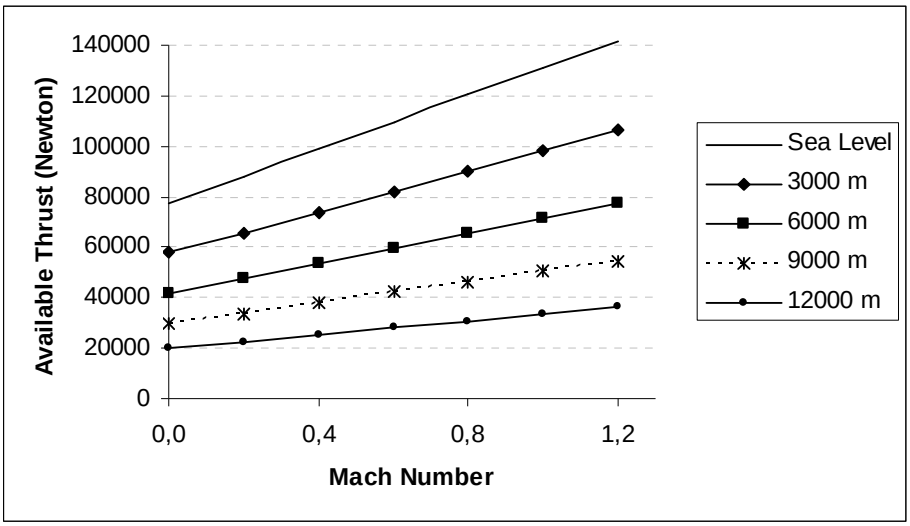

Figure 24.Maximum Available Thrust vs. Mach number

Note that, the available thrust values are obtained when the pilot applies full throttle setting, i.e. u = 1 and the afterburner is on. So, the maximum thrust will be less than that of represented when less throttle setting is applied. It can be seen from Figure 24 that flying at high altitudes will cause to gain less thrust force, so, this must be considered when performing evasive maneuvers.

b. Lift and Drag Forces

The lift force parameters of the fighter are approximated according to the Eqs. (12), (13), and (15). Note that the two dimensional lift curve slope at Mach=0 is an aircraft specific quantity and assumed to be 5.73 / ^{o}. The variation of lift coefficient curve slope by Mach number is shown in Table 2.

Table 2.The Variation of $c_{l\alpha}$

Mach Number	**Lift Coefficient Curve Slope, $c_{l\alpha}$, (per degree)**
0	5.73
0.2	5.84
0.4	6.25
0.7	8.02
1.2	6.03
1.4	4.08
1.8	2.67

By deriving the lift coefficient curve slope, the lift coefficient can be calculated at any Mach number for various angle of attack values. The lift coefficient variation is shown in Figure 25.

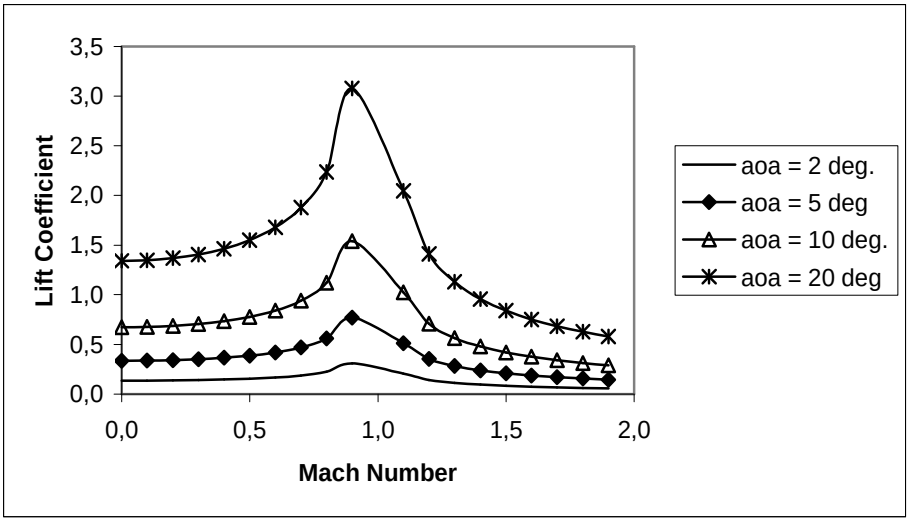

Figure 25.C_L vs. Mach Number for Different Angle of Attack Values

A fighter performing evasive maneuvers will probably fly at its corner speed which is 0.7 Mach in this case. Consequently, the lift coefficient curve of the fighter will be as shown in Figure 26. The lift coefficient for $\alpha = 0$, C_{L0} , is assumed to be zero.

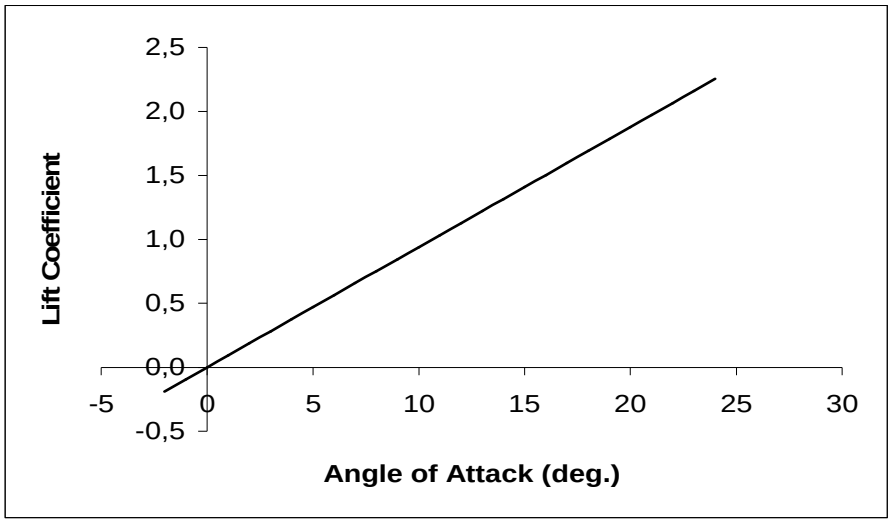

Figure 26.Lift coefficient – Angle of Attack Curve for M=0.7

As the lift coefficient increases linearly up to the maximum attainable angle of attack, the lift coefficient values in Figure 26 are calculated up to the stall angle of attack. The applied angle of attack variables are controlled at every time step of the simulation not to exceed the maximum value.

The parameters for approximating the drag coefficient at any altitude, speed, angle of attack are derived according mainly to the Eq. (16).

The zero-lift drag coefficient, C_{D_o} , is

$$C_{D_o} = C_f \frac{S_{wet}}{S} = 0.0035 \frac{138.89 \text{ m}^2}{27.870912 \text{ m}^2} = 0.0174 \qquad (71)$$

Note that, the wave drag, $C_{D_{wave}}$, which is assumed constant in this study, 0.0213, is added to C_{D_o} for Mach values exceeding Mach 1.

Oswald's efficiency factor, e_o, the value that is used to find the induced drag, C_{Di}, is calculated with the Eq. (22)

$$e_o = 4.61\,(1-0.045\,\mathcal{AR}^{0.68})\,(\cos\Lambda_{LE})^{0.15} - 3.1 \quad (72)$$

$$e_o = 4.61\,(1-0.045\,(4.08)^{0.68})\,(\cos 40^o)^{0.15} - 3.1 = 0.810 \quad (73)$$

For the subsonic regime, the k_1 value is derived with the Eq. (20):

$$k_1 = 1 / \pi\, e_o\, \mathcal{AR} = 1 / (3.14159 * 0.810 * 4.08) = 0.096 \quad (74)$$

And, the k_1 value for the supersonic regime varies with the Mach number. For instance, at Mach number, $\mathcal{M} = 1.2$, the k_1 value can be calculated with the Eq. (21):

$$k_1 = [\,[4.08 * ((1.2)^2 - 1)] / [(4 * 4.08 * \sqrt{(1.2)^2 - 1}) - 2\,]\,] * \cos(40^o) \quad (75)$$

$$k_1 = 0.15582 \quad (76)$$

After deriving necessary parameters, the drag coefficient can be calculated at any altitude and the Mach number. Firstly, the effect of the lift coefficient on the drag polar is shown in Figure 27.

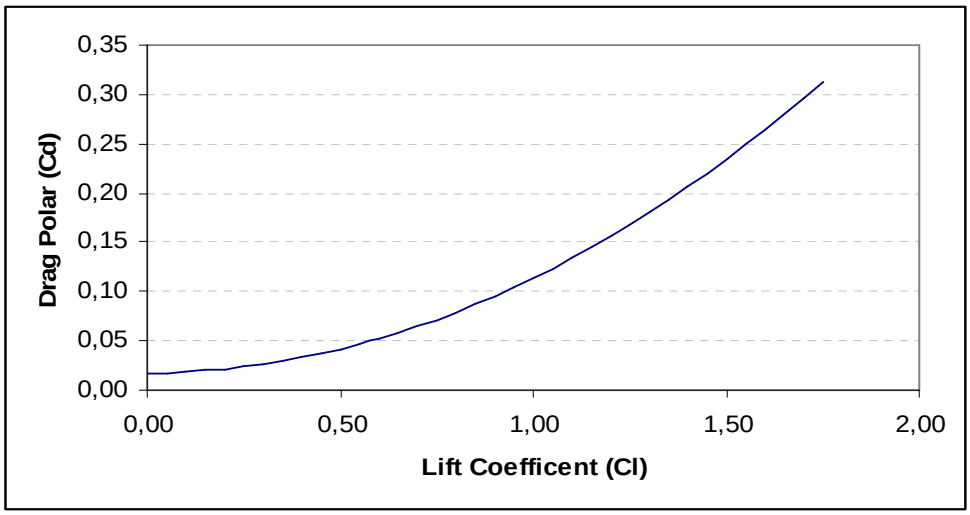

Figure 27.Effect of the Lift Coefficient on the Drag Polar

It is noted from the Figure 27 that the drag coefficient will increase by the square of the lift coefficient.

Table 3 represents the zero-lift drag coefficient, the k_1 factor, the induced drag coefficient, and the total drag polar for various Mach numbers when the angle of attack is 3^o, and Figure 28 represents variation of the total drag coefficient with the Mach number for different angle of attack values.

Table 3.Variation of Drag Coefficient ($\alpha = 3^o$)

Mach Number	C_{D_o}	k_1	$C_{D_i}=k_1 C_L^2$	$C_D = C_{D_o} + C_{D_i}$
0.2	0.0174	0.096	0.0018	0.0192
0.4	0.0174	0.096	0.002	0.0195
0.7	0.0174	0.096	0.0033	0.0208
1.2	0.0387	0.155	0.0031	0.0418
1.4	0.0387	0.214	0.0019	0.0407
1.8	0.0387	0.312	0.0012	0.0399

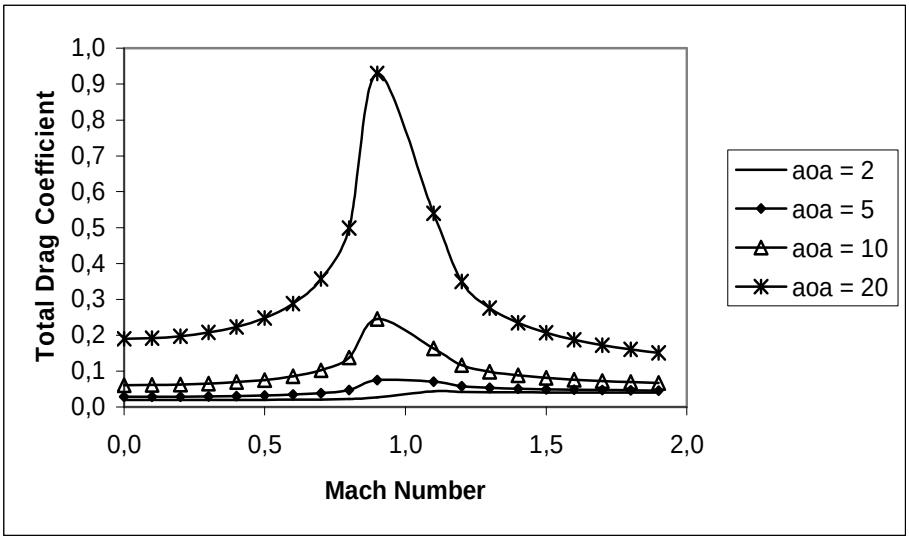

Figure 28. C_D vs. Mach Number for Different Angle of Attack Values.

By examining the figures 25 and 28, it can be seen that there are sudden changes in both the lift coefficient and the drag coefficient at the transonic regime. Transonic flow fields are too complex for accurate analysis by any but the most

advanced methods, and the analysis often requires hours of computing time on the fastest supercomputers for a single flight condition [26]. Because of that the transonic regime was not studied in this thesis.

B. MANEUVERING PERFORMANCE

1. Horizontal Turns

The most important metrics in aircraft performance are the turn radius and the turn rate. As mentioned in chapter 1, best turn performance for a specific aircraft is gained when it is at the corner speed. For fighters with high-g capability, the corner speed varies between 400 and 500 knots. After a number of experiments are conducted, it has been seen that the fighter model in the simulation has a corner speed of 447 knots, i.e. 230 m/sec, which nearly fits the corner speed of the actual F-16 fighter (450 knots).

Figure 29 represents the x and y positions for the fighter when it performs a 360-degree turn in the horizontal turn starting at the corner speed. The maximum applied angle of attack is adjusted at each time step in order to keep the load factor and the pitch rate in limits. The applied bank angle is 82.

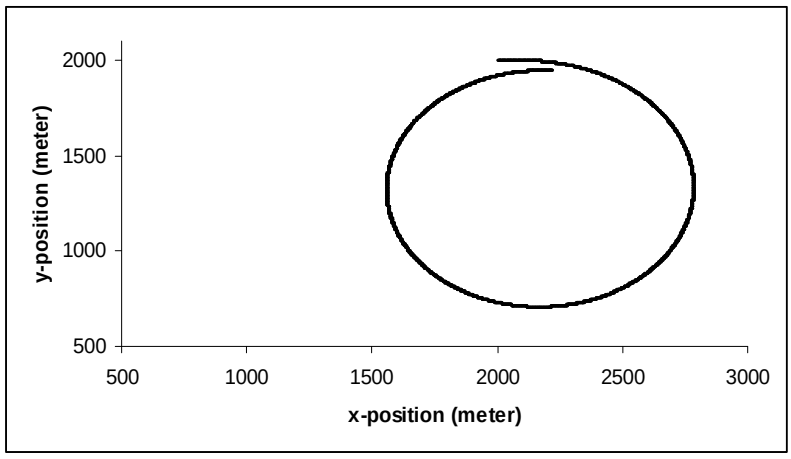

Figure 29.Trajectory in a Horizontal Turn (Upper View)

When the attitudes of the fighter in a horizontal turn are investigated, it is seen that the turn radius of the fighter is 630 meters, and the maximum load factor is 8.

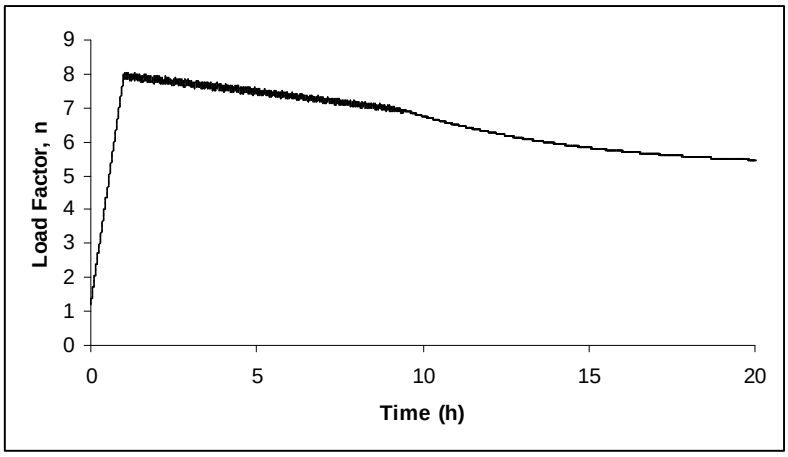

Figure 30.Load Factor Variation during the Horizontal Turn

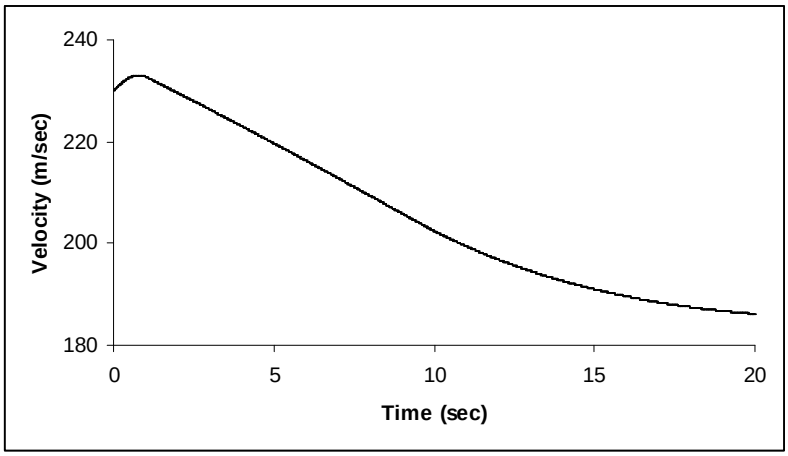

Figure 31.Velocity Variation during the Horizontal Turn

The speed of the fighter decreases because of the drag force. As the decrease in the velocity, the lift on the wings decreases and this causes the load factor to decrease. Figure 30 and 31 show the variation of the load factor and the velocity during the horizontal turn, respectively.

Thus, we can conclude that, before performing a turn, the initial speed must be adjusted correctly to keep the speed near the corner velocity for gaining higher turn performance.

2. Vertical Turns

As in the horizontal turn maneuver, satisfying results are obtained in a vertical turn maneuver. In the vertical turn maneuver, the fighter starts the maneuver 2000 meters from the origin in the x-axis, and has an altitude of 1000 meters. The applied angle of attack is controlled during the turn in order to maintain the g values of the aircraft below the structural limit of 9-g. The initial velocity of the aircraft is constant and 230 m/sec. Figure 32 represents the trajectory of the fighter during the turn maneuver in the vertical plane.

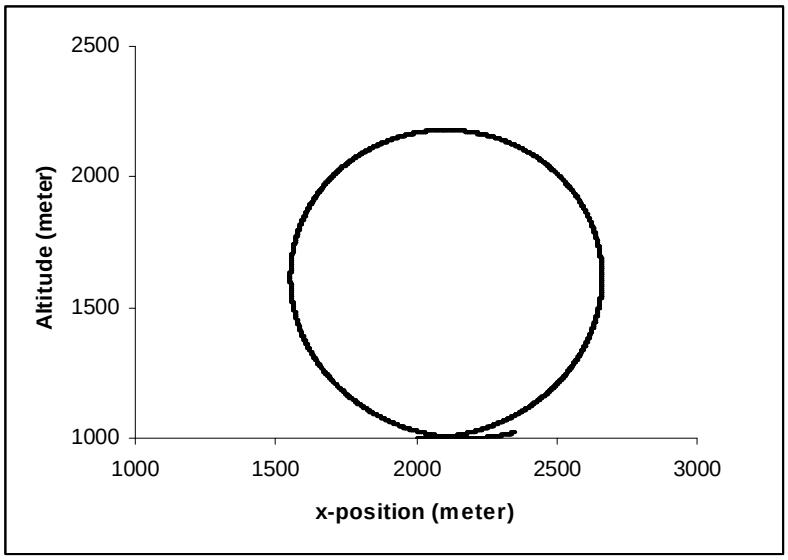

Figure 32.Trajectory in a Vertical Turn

It's observed that the turn radius of the fighter in the x-axis is 588 meters, and the turn radius in the z-axis is 638 meters. The difference in the radius values arise from the instantaneous velocities and the load factor values.

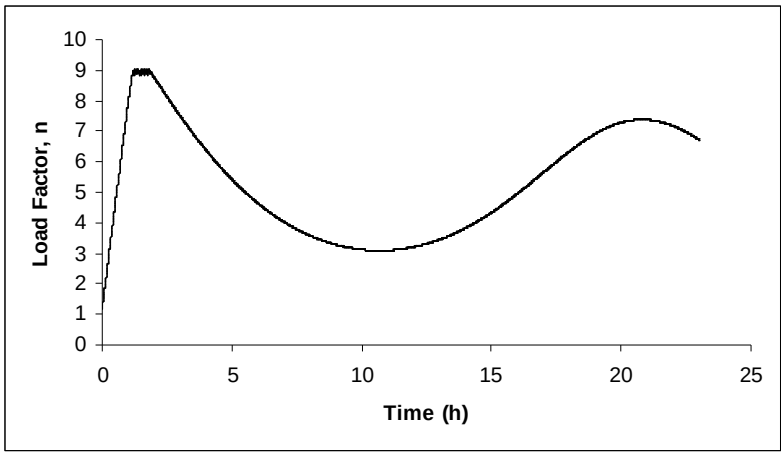

Figure 33.Load Factor Variation during the Vertical Turn

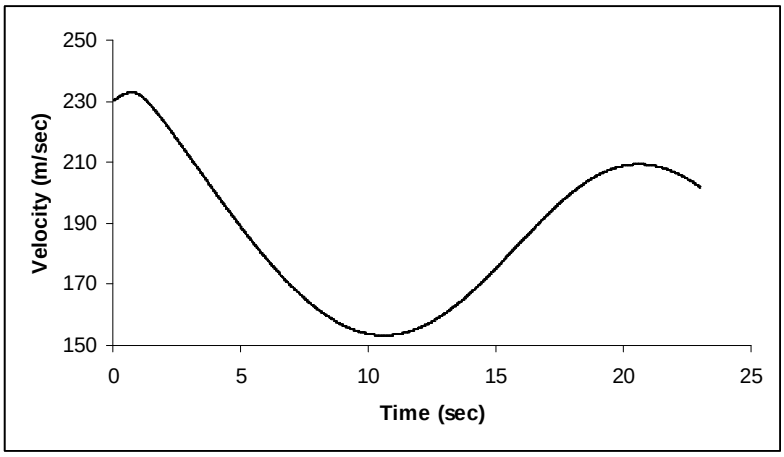

Figure 34.Velocity Variation during the Vertical Turn

Figure 33 and 34 represents the load factor and velocity variation during the vertical turn, respectively. The presented attitudes of the fighter make the shape of the circle seem like an ellipse. This shape is called a “tactical egg” [23].

The derived value, from Eq. 49, for the turn radius in a 9-g turn is 599 meters, and is agreeable with the obtained value from the simulation.

C. ENGAGEMENT SCENARIOS

In this section, the effectiveness of the evasive maneuvers performed by the fighter is measured. The performance metric is chosen as the flight time of the engagement scenario.

1. Scenario 1

In this engagement scenario, the initial positions and the velocities of the vehicles are fixed. The initial values for the scenario 1 are as follows.

$x_m = 0$ m. $y_m = 0$ m. $z_m = 1000$ m. $V_m = 1000$ m/sn

$x_t = 9000$ m. $y_t = 0$ m. $z_t = 5000$ m. $V_t = 300$ m/sn

Both the missile and the target take level flight initially. The heading angle of the missile varies from -45^o to $+45^o$ with the interval of 15^o, and the heading angle of the fighter from 0^o to 180^o with the same interval.

Figures 35-39 show the resulting flight times for different evasive maneuvers. The mark "*" denotes "failure" of the missile for that initial heading angle, χ_m . Note that, "failure" of the missile is the "success" of the fighter.

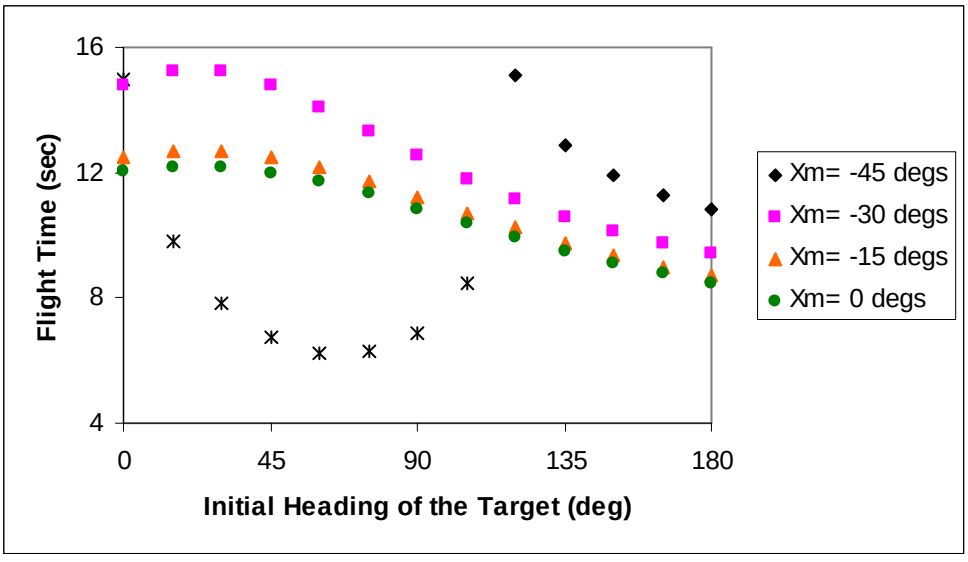

Figure 35.a.Flight Time (Horizontal-s)

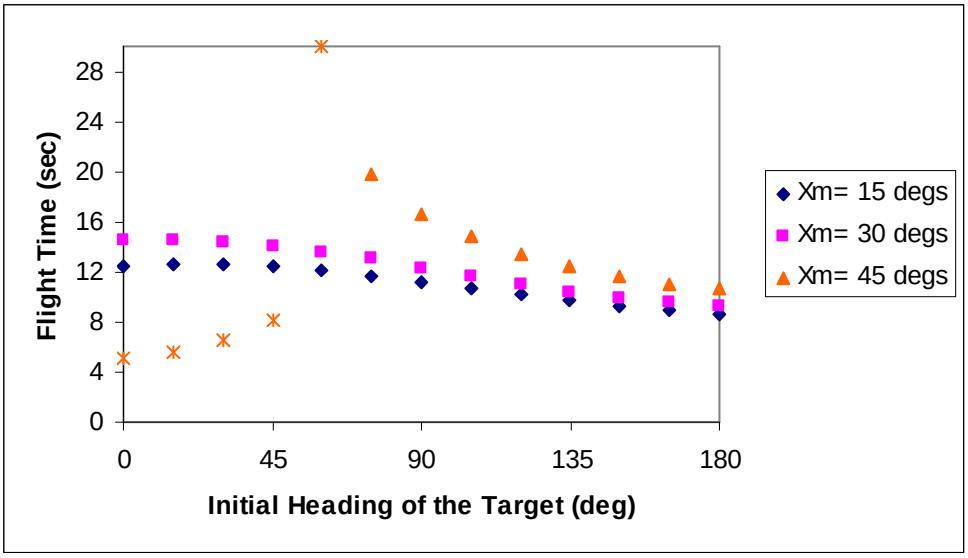

Figure 35.b.Flight Time (Horizontal-s)

In horizontal s maneuver, the fighter maneuvers so that it draws a virtual "S" in the sky and then continues level flight. It doesn't keep on turning horizontally after it finishes that virtual "S", because it loses speed significantly while turning. So, it has to gain speed after the horizontal s maneuver.

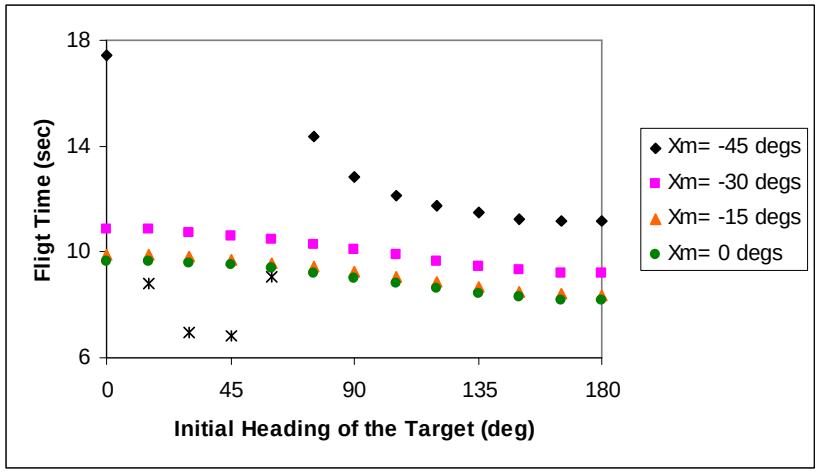

Figure 36.a.Flight Time (Split-s)

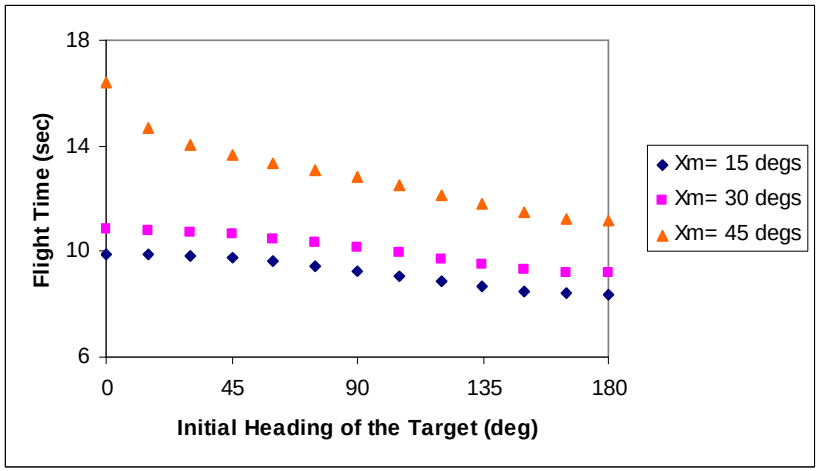

Figure 36.b.Flight Time (Split-s)

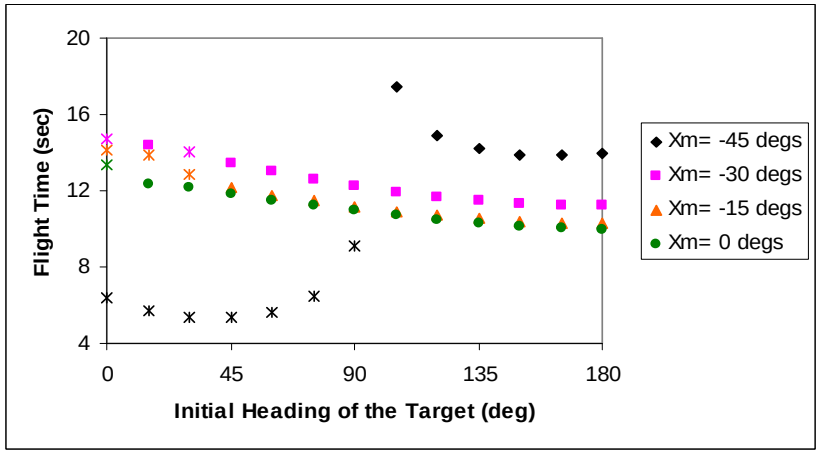

Figure 37.a.Flight Time (Immelmann)

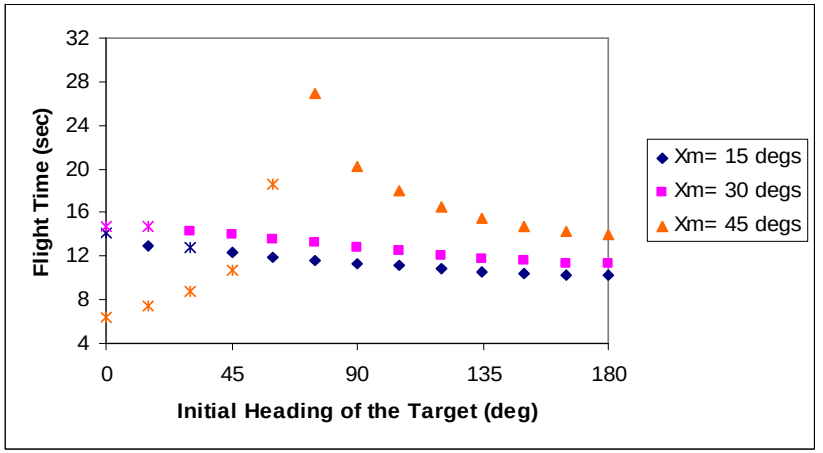

Figure 37.b.Flight Time (Immelmann)

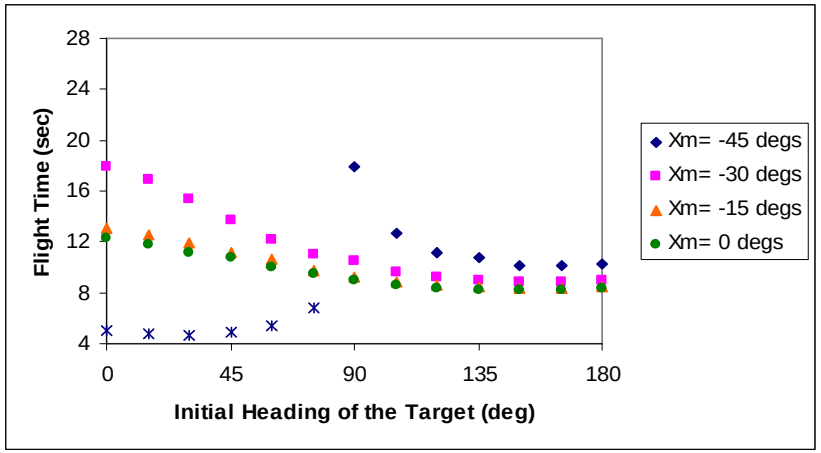

Figure 38.a.Flight Time (Barrel Roll)

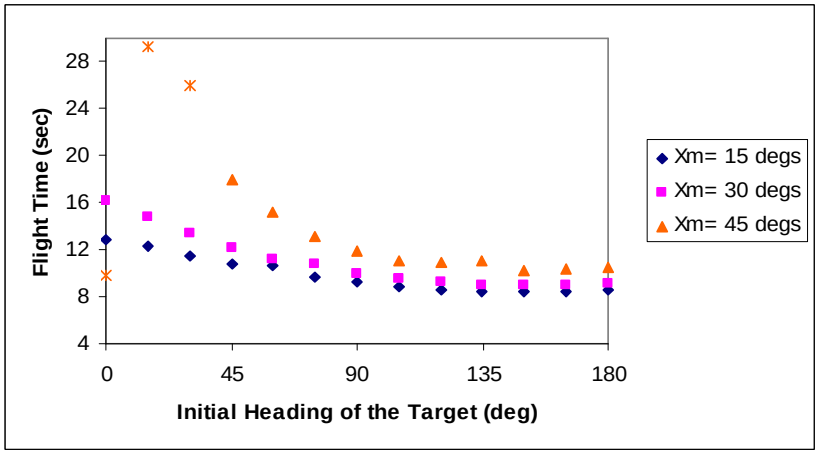

Figure 38.b.Flight Time (Barrel Roll)

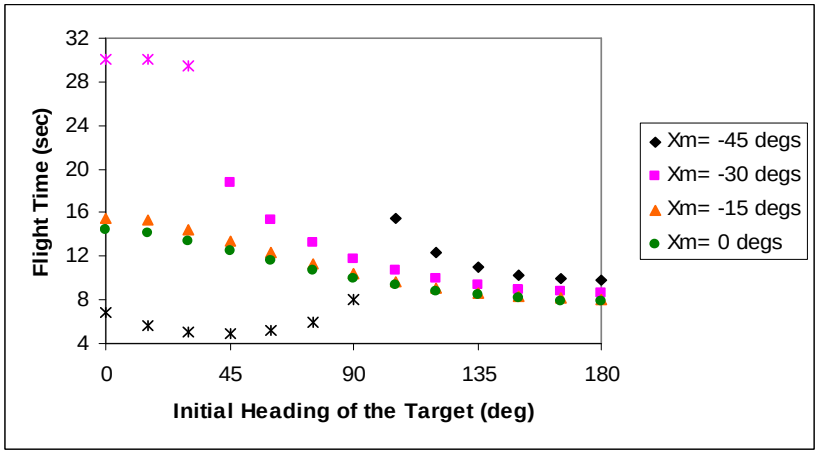

Figure 39.a.Flight Time (Linear Acceleration)

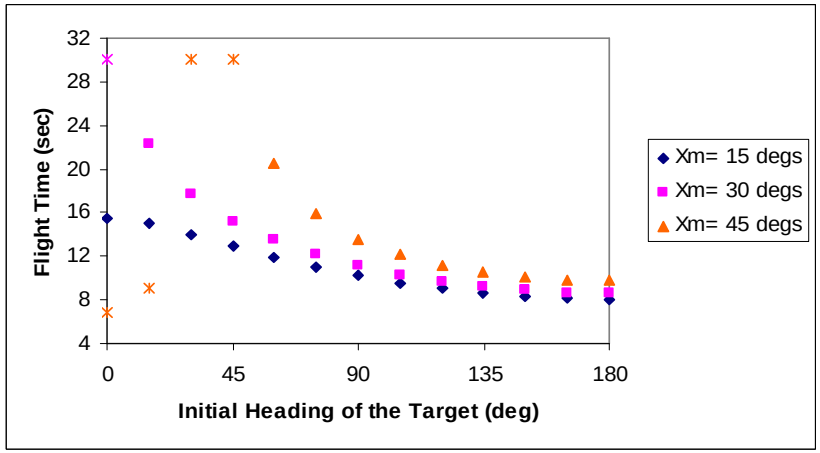

Figure 39.b.Flight Time (Linear Acceleration)

When the Figures 35-39 are examined;

In cases when “failure” occurs, it’s observed that the missile’s seeker look angle exceeds 90 degrees, so the missile can no more follow the fighter. In most cases, the missile fails to capture the fighter when its initial heading is -45^{o} and $+45^{o}$.

In a few cases, the fighter can succeed in evasion -other than the initial headings of the missile, -45^{o} and $+45^{o}$- when it performs the Immelmann maneuver. This is the expected result, because of the initial displacements of the vehicles in the vertical plane. The fighter starts maneuvering 4000 m. above the missile, and in the Immelmann maneuver, the fighter performs a vertical climb. After 10 seconds from the beginning of the scenario, the missile runs out of fuel and thrust. Consequently, the missile starts to lose its speed rapidly as it goes on climbing to chase the fighter, and at last, it fails to capture the target.

The other exceptional evasion tactic for these initial conditions is the linear acceleration. The fighter doesn’t perform any evasive turn; it just keeps on level flight. If the initial heading of the fighter is so that it goes far away from the missile, it may manage to evade from the missile. Because, in such cases, it keeps its altitude at 5000 meters, and goes far from the missile. Thus, the fuel of the missile completely burns before it captures the fighter, and its speed starts to decrease. Finally, it fails to capture the target.

For the cases where the fighter is captured, the evasive maneuvers in regard of the average flight times are compared, and the results are represented in Table 4.

Table 4.Average Flight Times for Scenario 1

Maneuver	**Average Flight Time (sec)**
Horizontal s	11.80
Split s	10.33
Immelmann	12.55
Barrel Roll	10.77
Linear Acceleration	11.43

It is seen from Table 4 that the Immelmann maneuver proves more time, in average, to escape from the missile than the others. Also, long average flight time is obtained when the evasive maneuver is the horizontal-s maneuver.

In general, it's noted that, if the initial altitude of the fighter is higher than that of the missile, maneuvers which makes the fighter go higher and far away from the missile provide more chance to evade from the missile, and increases the flight time of the engagement.

2. Scenario 2

In this scenario, the initial positions of the vehicles are fixed. But, this time the altitude of the missile is some hundred meters higher than the fighter's. The initial conditions are as follows:

$x_m = 0$ m. $y_m = 0$ m. $z_m = 3300$ m.

$V_m = 950$ m/sn $\chi_m = 0^o$

$x_t = 8000$ m. $y_t = 0$ m. $z_t = 3000$ m.

$V_t = 240..300$ m/sn $\chi_t = 0^o..180^o$

Both vehicles take level flight initially. The heading angle of the missile is fixed. The velocity of the fighter varies from 240 m/sn to 300 m/sn with the interval of 20 m/sn. For each initial velocity of the target, its heading angle varies from 0^o to 180^o with the interval of 5^o. By given vehicle coordinates

The results of this scenario are represented in Figures (40-43).

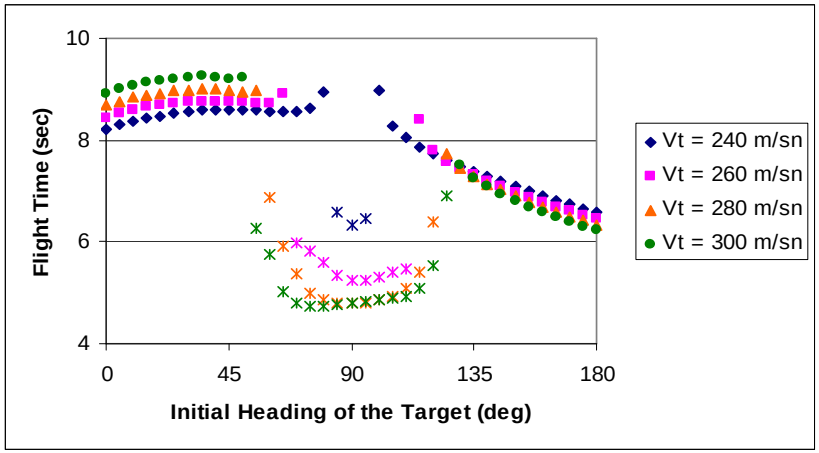

Figure 40.Flight Time for Scenario 2 (Horizontal-s)

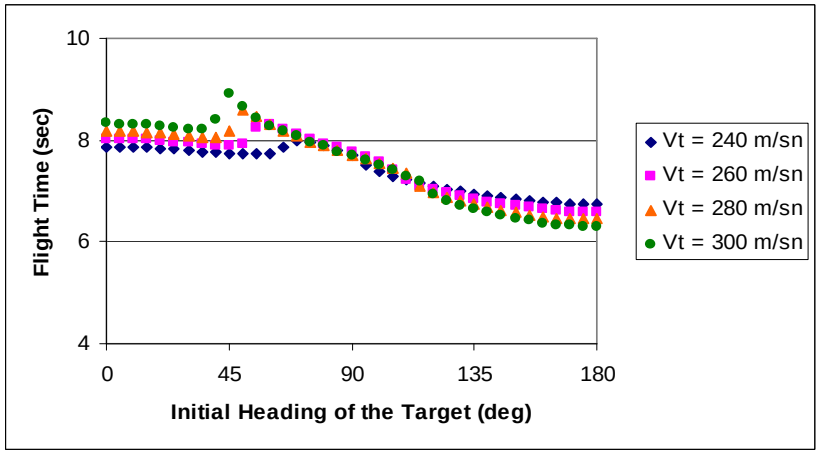

Figure 41.Flight Time for Scenario 2 (Split-s)

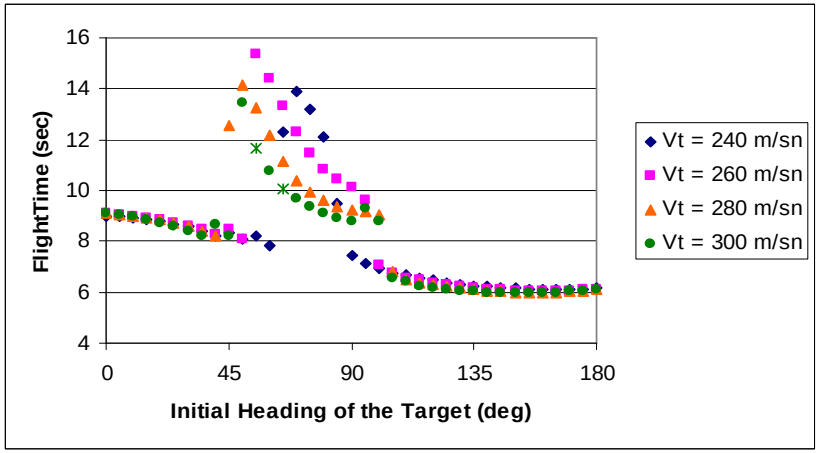

Figure 42.Flight Time for Scenario 2 (Barrel Roll)

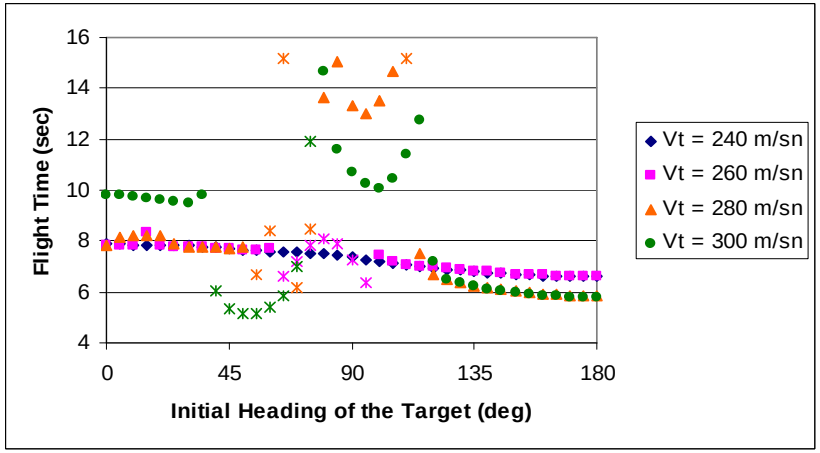

Figure 43.Flight Time for Scenario 2 (Immelmann)

It’s noted from the figures that the initial heading of the fighter makes significant changes on the flight time for the cases which the missile achieves to hit the fighter. For instance, when the fighter performs horizontal-s maneuver, initial heading angles which makes fighter go far from the missile, i.e. $0^o<\chi_t<90^o$, favor flight time for the fighter. On the other hand, the resulting flight time values decrease as the fighter is oriented towards the missile.

It’s also noted that, in general, higher initial velocities causes the flight time to increase only when the initial heading of the fighter is between 0 and 90 degrees. For initial heading angle values exceeding 90 degrees, lower initial velocities seem to obtain better flight time results for the fighter.

The most noteworthy point for this scenario is the flight time values when the initial heading angles are near 90 degrees. In this case, almost every maneuver, except the split-s, causes very high flight time values, and proves avoidance from the missile. The best performance is obtained by the horizontal-s maneuver. Although the Immelmann maneuver also causes long flight times, it rarely makes the fighter manage to avoid from the missile compared to the horizontal-s. It’s also seen that higher initial velocities favors evasion performance in these situations.

The barrel roll maneuver is seemed noteworthy due to its efficiency between 45 and 90 degrees. By performing this maneuver, long flight times are obtained for any of the initial velocities. It has been seen that this maneuver may be performed at any initial speed to gain time when the initial headings are between 45 and 90 degrees.

Note that the initial heading of the missile is 0^o in all cases of the scenario 2. It means that its heading is always towards the fighter regardless of its heading at the beginning of the engagement scenario. According to the proportional navigation guidance system, the missile steers towards the anticipated position of its target. Hence, the initial heading of the missiles is set to

+5^{o} and the flight time values are observed. Figure 44 represents the results under these conditions when the initial velocity of the fighter is 280 /sn.

As seen in Figure 44, if the initial heading angle of the missile is truly oriented towards the possible further positions of the fighter at the beginning of the terminal phase, survival chance of the fighter decreases to zero. Then, the flight time of the encounter becomes important for the fighter.

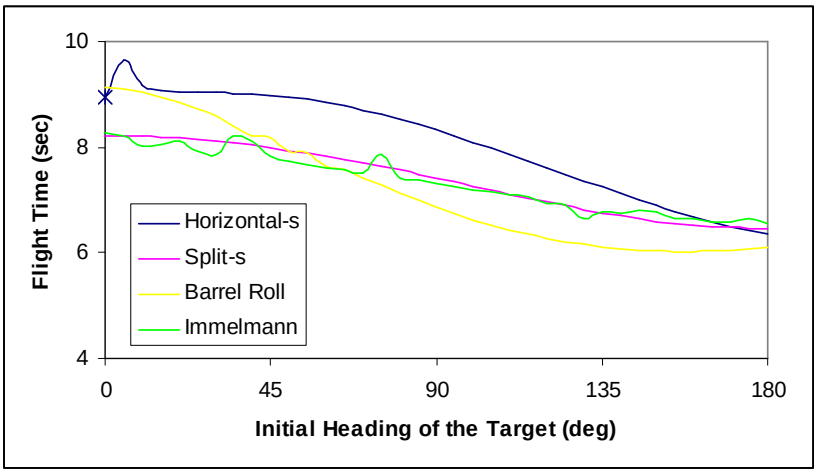

Figure 44.Flight Time (Initial $\chi_m = 5^o$)

It's noted from Figure 44 that the fighter gives the hardest guidance problem to the missile when it performs a horizontal-s maneuver.

The split-s and the Immelmann seem identical, and the flight times obtained with these two maneuvers vary between 8.29 and 6.47 seconds.

By performing the barrel roll maneuver, better results than the Immelmann and the split-s are obtained for the initial heading angles not exceeding +55^{o}. It's observed that the initial heading angles beyond +55^{o} decreases evasion performance of the fighter.

Consequently, under given conditions, it can be concluded that the horizontal-s maneuver is the most convenient evasive maneuver against proportional navigation when we take the flight time as the performance metric.

All the figures that are represented for the scenario 2 show another important fact. If the headings of the vehicles are towards each other initially, none of the evasive maneuvers that the fighter performs can change the flight time significantly. So, a fighter pilot must try not to fall in such a positional geometry.

3. Scenario 3

In this section, the methods for improving the efficiency of some of the evasive maneuvers are studied. The initial positions of the vehicles are 0, 0, 3000 for the missile and 9000, 0, 7000 for the fighter. The initial velocities are 950 m/sec for the missile and 240 m/sec for the fighter. The initial heading angles of the missile and the fighter are 0^o and 90^o, respectively. The fighter performs a horizontal-s maneuver with 8 g. The trajectory of this engagement in all planes is shown in Figures 45-47.

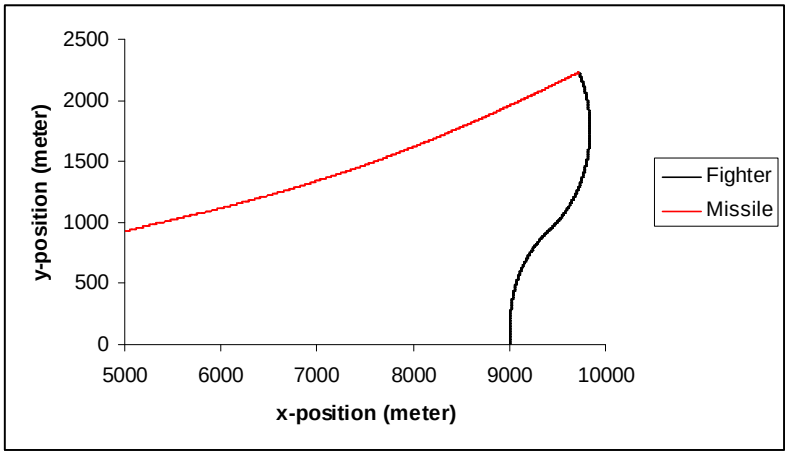

Figure 45.Vehicle Trajectories in the x-y Plane for Scenario 3

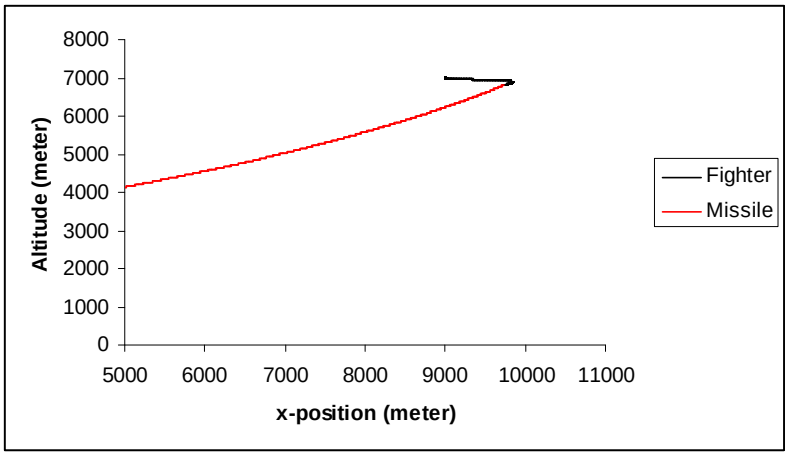

Figure 46.Vehicle Trajectories in the x-z Plane for Scenario 3

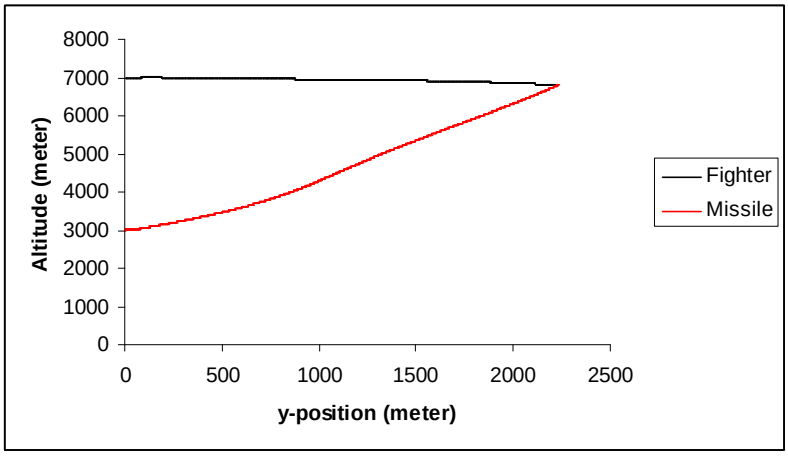

Figure 47.Vehicle Trajectories in the y-z Plane for Scenario 3

When the fighter performs a horizontal-s maneuver with hard turns, the fighter loses its velocity considerably. Thus, the fighter will be in danger although it manages to evade the missile because of possible further threats. If such a situation is not desired, the g's that the fighter pulling, i.e. the load factor, n, must be decreased. Figure 48 represents the velocity history of the fighter when it performs horizontal-s maneuver with different load factors.

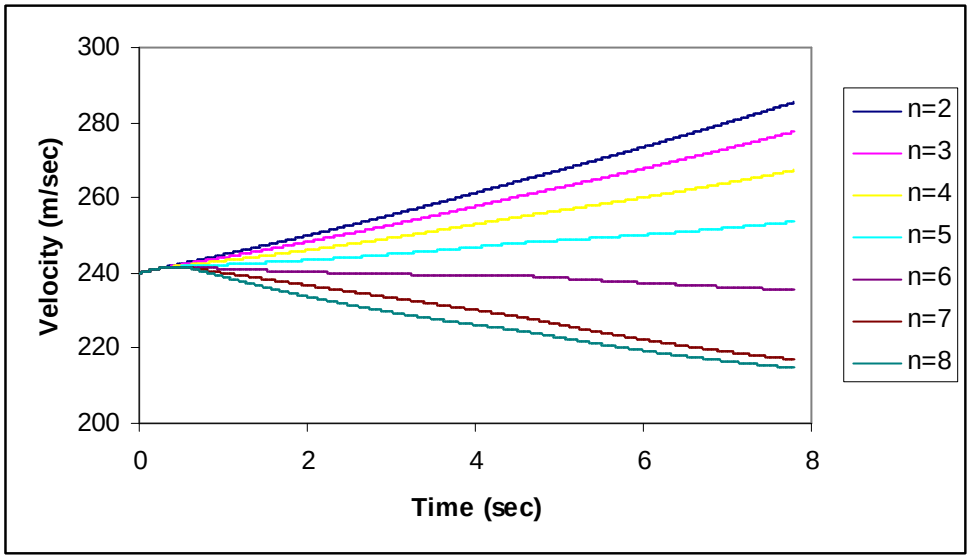

Figure 48.Velocity History of the Fighter for Horizontal-s Maneuver

It's noted from Figure 48 that the velocity of the fighter decreases significantly as it performs harder turns. When the aerodynamic forces during the maneuver are observed, it is seen that the drag force has the greatest effect on this velocity dissipation. The fighter applies more angle of attack to make a harder turn; this causes the lift coefficient to rise and triggers the induced drag coefficient. Finally, total drag polar increases and the velocity of the fighter decreases.

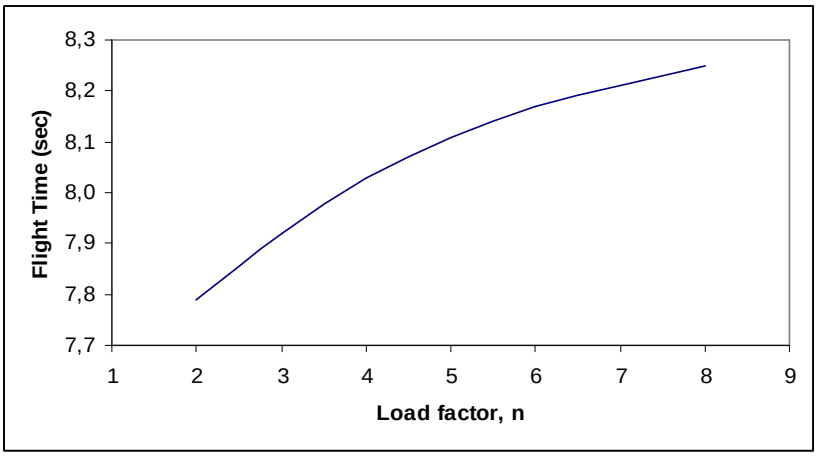

Figure 49.Effect of Load Factor on the Flight Time (Horizontal-s)

At this point, a trade-off between the velocity and the flight time occurs. Lower load factors in horizontal-s maneuver occasions the flight time to be

shorter. Namely, if it is desired to maintain the initial velocity during the maneuver, lower load factors -which will shorten the flight time- must be applied. According to the tactical situation, the pilot must make a critical decision considering this fact. In Figure 49, the effect of the load factor on the flight time is shown.

When the barrel roll maneuver is observed, it's noted that this maneuver is more effective than the horizontal-s maneuver when the maintenance of the velocity is desired. Figure 50 shows the velocity comparison of these two maneuvers in a 10-second engagement.

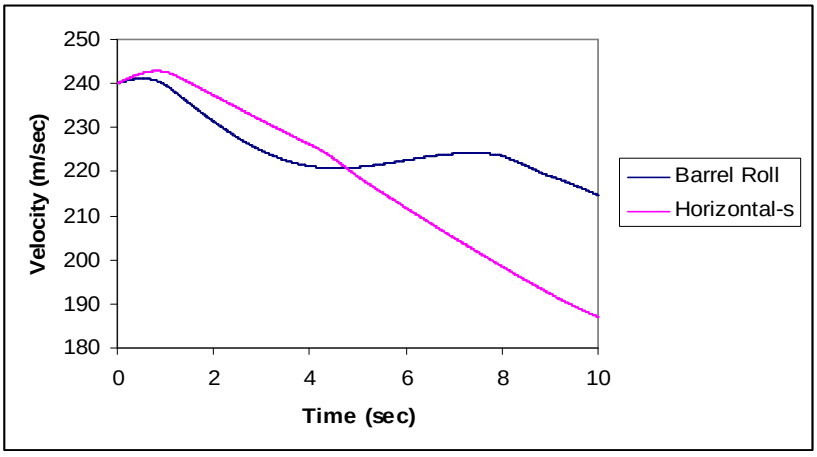

Figure 50.Velocity Comparison of Barrel Roll and Horizontal-s

When we think of an air combat as a whole, keeping the velocity near the corner velocity will favor further evasive maneuvers which require consequent turns. Then, the barrel roll maneuver is an effective maneuver when this fact is considered. Also, it's observed that performing barrel roll when the altitude of the fighter is higher than the missile will be convenient for better evasion performance.

The performance of the barrel roll maneuver can be improved by some corrections on the applied bank angle and angle of attack values. In barrel roll maneuver whose velocity variation is shown in Figure 50, the maximum applied angle of attack is 15 degrees, and the bank angle rate is 45 degrees/sec. These values cause the fighter to draw a virtual "barrel" with low radius. It can be seen

from Figure 50 that the velocity of the fighter decreases from 240 m/sec to 214 m/sec. The difference is 26 m/sec and equal to 93 km/hour (state 1). To prevent this velocity dissipation, the maximum applied angle of attack is reduced to 10 degrees, and the bank angle rate is reduced to 30 degree/sec (state 2). In Figure 51, the velocity comparison of these two barrel roll applications is shown.

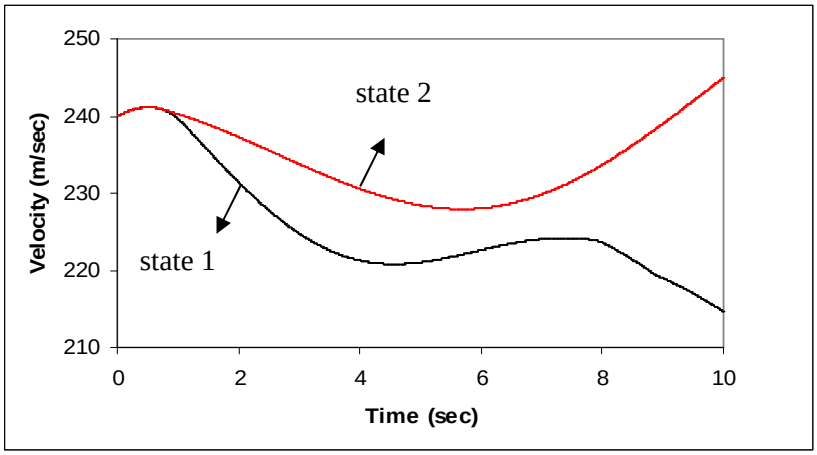

Figure 51.Velocity Comparison of Two Barrel Roll Maneuver Application

For a detailed study on barrel roll maneuver which considers it from an optimal view, see [37].

By altering the applied commands on the barrel roll maneuver, it is also seen that the evasion performance of the fighter doesn't decrease significantly. Moreover, it proves longer flight times for the fighter in some cases. With the initial conditions of scenario 3, we examine the flight times when performing a barrel roll maneuver. Figure 52 represents the flight time values for initial heading angles between 0^o and 180^o with the interval of 15^o.

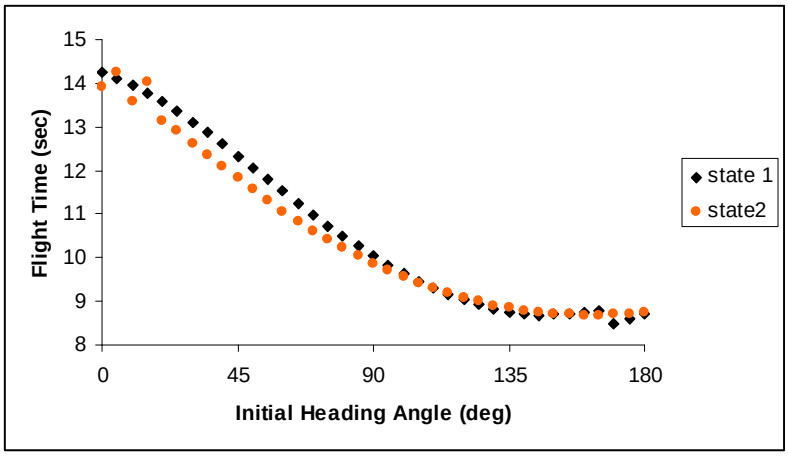

Figure 52.Flight Time Comparison for Two Barrel Roll Maneuver Application

D. PARAMETER RECORDS OF AN EVASIVE MANEUVER

In this section, we intend to show that the fighter model in this study is agreeable with the aircraft-specific limitations. A high-g horizontal-s maneuver that coerces the limits is chosen.

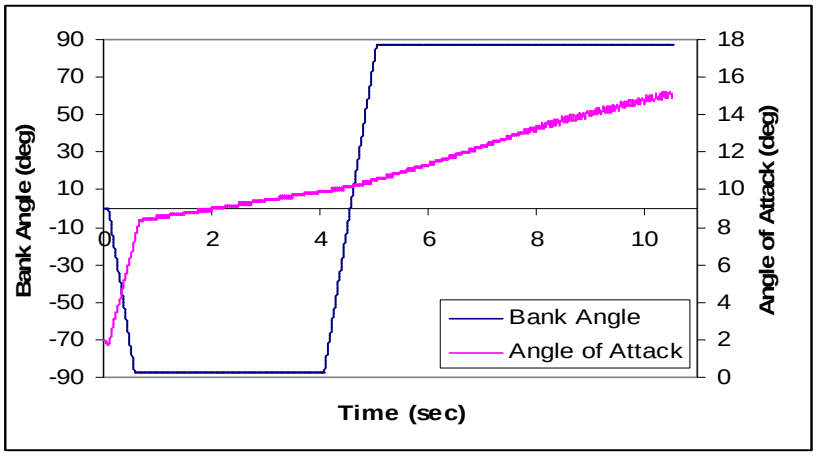

Figure 53.Bank Angle and Angle of Attack History for Horizontal-s Maneuver

In the simulations, the bank angle is applied so that the roll rate of the fighter never exceeds 180 degree/second. This value fits with the roll rate values of the contemporary fighters. The excepted values are between 100^{o} and 200^{o} [11]. The angle of attack rate is also controlled at each time step in order to hold the pitch rate under the excepted value, i.e. 20 degree/second for a modern fighter [11]. The pitch rate value is derived by the following equation:

$$\boldsymbol{P} = \dot{\alpha} + (\dot{\Upsilon} * \cos(\mu)) + (\dot{\chi} * \cos(\Upsilon) * \sin(\mu)) \quad (77)$$

Figure 53 represents the bank angle and angle of attack history, and Figure 54 represents the pitch rate history during the maneuver.

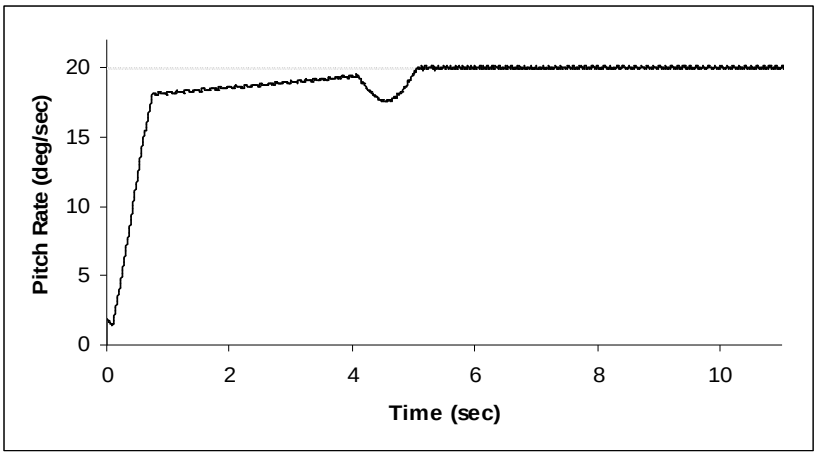

Figure54.Pitch Rate History for Horizontal-s Maneuver

Another important limitation for the fighter is the load factor. During the maneuver, the load factor must not exceed the aircraft-specific quantity. A load factor limit of 9-g is chosen for the fighter that's modeled in this study. The history of this value is shown in Figure 55.

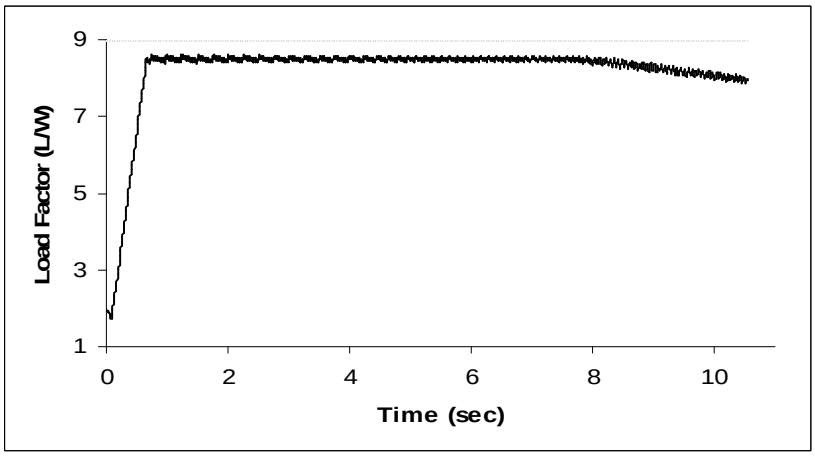

Figure55.Load Factor History for Horizontal-s Maneuver

As it is mentioned in chapter 2, lift-to-drag ratio is an important parameter for an aircraft. Maximum value for this parameter is 10-25 for a fighter at subsonic speeds. The calculated lift-to-drag ratio values for the horizontal-s maneuver are shown in Figure 56.

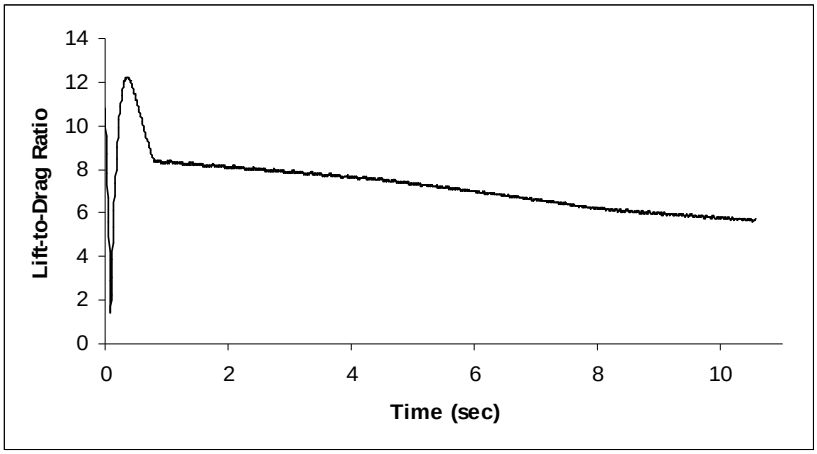

Figure56.Lift-to-Drag Ratio Values during Horizontal-s Maneuver

V.CONCLUSION

In an air combat, the maneuvers performed by the fighters are of crucial importance. Understanding the current tactical situation, choosing the convenient maneuver, applying correct commands are vital matters for a fighter pilot. Especially, when an incoming missile is detected, a pilot has very few seconds to think and to make a move. So, he must know the characteristics, the limitations and the abilities of his fighter. This is only possible with training. As practicing the maneuvers with real fighters are very expensive and time consuming task, it is inevitable to model realistic fighters and to simulate their maneuvers with computers. Namely, a pilot must know what may happen where and when he performs an evasive maneuver before he takes off for a mission. It will be invaluable for an air force whose pilots are illuminated with this knowledge.

In this thesis, a realistic 3D model of a fighter and the evasive maneuvers performed against missiles which employ one of widely used guidance systems, proportional navigation, are evaluated via software. With this software that is developed by us, supplying it with the required aircraft-specific data and with the initial conditions, it is possible to analyze the attitudes of that aircraft when it performs different maneuvers, or analyze the performance of its evasive maneuvers against a proportional navigation.

By the simulation runs that have been conducted, it is noted that the performance of a particular evasive maneuver may vary according to the initial positional geometry. The performance can be improved by making some changes to applied commands which will change the turn radius, the load factor, and the velocity, etc. of the fighter. It is also noted that there are significant effects of aerodynamic forces on the attitudes of the fighter.

The modular structure of the software makes it easy to understand, and apt to further improvements. It is thought that, this work may be used by pilot training associations for training purposes, may be used as a medium to analysis the

performance of any kind of aircraft, and in the future, may be attached to a joint combat simulation which includes air, navy, army combat.

The followings can be stated as the future work:

- Addition of more fighters to the simulation,
- Development of novel algorithms for optimizing the evasion trajectory of a fighter,
- Implementation of an autopilot which will take the control of the fighter when a incoming missile is detected.

Finally, it was anticipated that; participating in the knowledge-sharing community in aeronautics domain as Turkish engineers will contribute our country to keep up with the latest developments and technologies.

REFERENCES

[1] Zarchan, P., *"Tactical and Strategic Missile Guidance"*, American Institute of Aeronautics and Astronautics, Vol. 199, Fourth Edition, 2002.

[2] Moran, I., *"Three Plane Approach for 3D True Proportional Navigation"*, Master Thesis, Naval Science and Engineering Institute, Istanbul, 2005.

[3] Gordon, D.F., Grefenstette, J.J., *"Explanations of Empirically Derived Reactive Plans"*, Proceedings of the Seventh International Conference on Machine Learning, pp. 198-203, Austin, TX, 1990.

[4] Moran, I., Altilar, D.T., *"Three Plane Approach for 3D True Proportional Navigation"*, AIAA Guidance, Navigation, and Control Conference, San Francisco, CA, August 2005.

[5] Choi, H.L., Bang, H.C., Tahk, M.J., *"Co-Evolutionary Optimization of Three Dimensional Target Evasive Maneuver against a Proportionally Guided Missile"*, Proceedings of the IEEE Congress on Evolutionary Computation, Vol.2, pp. 1406-1413, Seoul, Korea, May 2001.

[6] Ben-Asher, J., Cliff, E.M., *"Optimal Evasion against a Proportionally Guided Pursuer"*, Journal of Guidance, Control and Dynamics, Vol.12, No.4, pp.598-601, 1989.

[7] Imado, F. and Miwa, S., *"Fighter Evasive Maneuvers against Proportional Navigation Missiles"*, Journal of Aircraft, Vol.23, No.11, pp. 825-830, 1986.

[8] Imado, F., Uehara, S., *"Proportional Navigation Versus High-G Barrel Roll Maneuvers From Optimal Control of View"*, AIAA Guidance, Navigation and Control Conference, 1996.

[9] Virtanen, K., Ethamo, H., Raivio, T., Hämäläinen, R.P., *"VIATO—Visual Interactive Aircraft Trajectory Optimization"*, IEEE Transactions on Systems, Man, and Cybernetics-Part C: Applications and Reviews, Vol.29, No.3, pp. 409-421, August 1999.

[10] Ong, S., and Pierson, B., *"Optimal Planar Evasive Aircraft Maneuvers against Proportional Navigating Missiles"*, Journal of Guidance, Control and Dynamics, Vol.19, No.6, pp.1210-1215, 1996.

[11] Raivio, T., Ranta, J., *"Optimal Missile Avoidance Trajectory Synthesis in the Endgame"*, AIAA Guidance, Navigation, and Control Conference and Exhibit, Monterey, CA, 5-8 August 2002.

[12] Moore, F.W., Garcia, O.N., *"A New Methodology for Optimizing Evasive Maneuvers Under Uncertainty in the Extended Two-Dimensional Pursuer/Evader Problem"*, Proceedings of the Ninth IEEE International Conference on Tools with Artificial Intelligence (ICTAI-97), pp. 278-285, Newport Beach, CA, USA, 1997.

[13] Imado, F., *"Some aspects of a realistic three dimensional pursuit-evasion game"* Journal of Guidance, Control, and Dynamics, Vol. 16, No. 2, pp. 289-293 , 1993.

[14] Imado, F., *"Some Practical Approaches to Pursuit-Evasion Dynamic Games"*, Cybernetics and Systems Analysis, Vol. 38, No. 2, pp. 276-291, 2002.

[15] Norlin, K.A., *"Flight Simulation Software at NASA Dryden Flight Research Center"*, NASA Technical Memorandum 104315, October 1995.

[16] Burgin, G.H., Sidor, L.B., *"Rule-Based Air Combat Simulation"*, NASA Contractor Report 4160, September 1988.

[17] US Air Force, *"Flying Training and Ground Training for Pilots"*, 419 FW Instruction 11-401, 1997.

[18] Smith,R.E., Dike, B.A., Ravichandran, B., El-Fallah, A., Mehra, R.K., *"Discovering Novel Fighter Combat Maneuvers in Simulation: Simulating Test Pilot Creativity"*, In P. J. Bentley and D. W. Corne (Editors), Creative Evolutionary Systems, pp. 467-486., Morgan Kaufmann Publishers Inc., San Francisco, CA, 2001.

[19] *"Wide-Envelope Maneuvering and Upset Recovery Program Course Notes"*, Flight Emergency & Advanced Maneuvers Training, Inc. dba Flightlab, www.flightlab.net, available in July 2005.

[20] Crenshaw, D., *"How to Live and Die in the Virtual Sky"*, www.saunalahti.fi/~fta/acmintro.htm, available in July 2005.

[21] Newman, S., Whatley, D., Anderson, I., *"Engineering Design Education – The Integration of Disciplines"*, Aircraft Engineering and Aerospace Technology: An International Journal, Volume 75, No.1, pp. 18-26, Emerald Group Publishing Limited, February 2003.

[22] Andriambololona, M., Lefeuvre, P., *"Implementing a Dogfight Artificial Pilot"*, Research Report DKS03-07/ICE 07, Data and Knowledge Systems Group, Faculty of Information Technology and Systems, Delft University of Technology, Version 0.9, July 2003.

[23] Shaw, R.L., *"Fighter Combat: Tactics and Maneuvering"*, Naval Institute Press, Annapolis, Maryland, 1985.

[24] Karelahti, J., Virtanen, K., Raivio, T., *"Game Optimal Support Time of a Medium Range Air-to-Air Missile"*, Eleventh International Symposium on Dynamic Games and Applications, Tucson, AZ, December 2004.

[25] *http://www.combataircraft.com/tactics/the_immelman.asp*, available in July 2005.

[26] Brandt, S.A., Bertin, J.J., Stiles, R.J., Whitford, R., *"Introduction to Aeronautics: A Design Perspective"*, American Institute of Aeronautics and Astronautics, 1997.

[27] Scott, J., *"Atmospheric Pressure "*, www.aerospaceweb.org, 2001, available in July 2005.

[28] Miele, A., *"Flight Mechanics"*, Addison Wesley, Massachusetts, MA, 1962.

[29] Kim, S., Murphy, P.C., Klein, V., *"Evaluation and Analysis of F-16XL Wind Tunnel Data from Static and Dynamic Tests"*, Technical Memorandum, NASA/TM-2004-213234, NASA Langley Research Center, June 2004.

[30] Scott, J., *"Lift Coefficient & Thin Airfoil Theory"*, www.aerospaceweb.org, 2003, available in July 2005.

[31] Scott, J., *"Drag Coefficient & Lifting Line Theory"*, www.aerospaceweb.org, 2004, available in July 2005.

[32] Durham, B., *"Coordinate Systems"*, Department of Aerospace and Ocean Engineering, Virginia Tech, www.aoe.vt.edu/~durham/AOE5214, 2004, available in July 2005.

[33] Bairstow, L., *"Applied Aerodynamics"*, Longmans, Green and Co., 1939.

[34] Jackie Neider, Tom Davis, and Mason Woo, *"OpenGL Programming Guide"*, Reading, MA: Addison-Wesley Publishing Company, Second Edition, 1997.

[35] *"F-16 Fighting Falcon Multi Role Fighter"* www.aerospaceweb.org/aircraft/fighter/f16, available in July 2005.

[36] "*F-16 Fighting Falcon*" , www.globalsecurity.org/military/systems/aircraft/f-16-specs.htm, available in July 2005.

[37] Takano, H., Baba, Y., *"Optimal Flight Trajectory and Aerobatic Maneuvers Against Missiles"*, Proceedings of the 5th Asian Control Conference, Melbourne, Australia, July 2004.

APPENDIX-1: PUBLICATIONS

1. Akdağ, R., Altılar, D.T., *"A Comparative Study on Practical Evasive Maneuvers against Proportional Navigation Missiles"*, AIAA Guidance, Navigation and Control Conference, San Francisco, CA, 15-18 August 2005.